

8-7430-1-3719  
05 June 2002

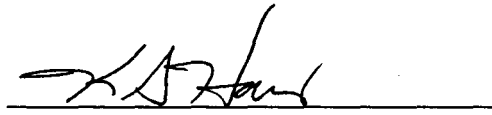
To: S. Siglin P10-44

Cc: J. Keller P32-31  
K. Landis P32-31

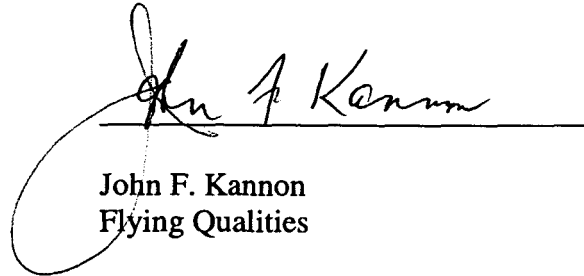
Subject: Delivery of BH Sim and B-29 Descriptions for U.K. RAF HC Mk2 Mull of Kintyre Accident Investigation

Attachment: 1) Simulation Math Model Description for the RAF HC Mk2  
2) Description of Tandem Helicopter Transient Analysis Program B-29

The purpose of this memorandum is to record the delivery of the documents containing the descriptions of the simulation math model and transient analysis program used in the analysis of the U.K. RAF HC Mk2 Mull of Kintyre accident investigation.



Kenneth S. Harris  
Flying Qualities



John F. Kannon  
Flying Qualities

## **ABSTRACT**

This document presents an overview of the major mathematical calculations and engineering physical equations used to represent the RAF HC MK2. This mathematical model is suitable for off-line and piloted simulation studies of the handling qualities of the RAF HC MK2. It is a total force, full flight envelope, six-degree-of-freedom tandem rotor helicopter model, which uses either a Fourier or a blade element approach to rotor modeling, based on user specifications. It has currently been implemented for execution on the Silicon Graphics Challenge and Onyx family of computers. With recompilation, it can be configured to run on other platforms.

## **KEY WORDS**

Aerodynamics  
Aircraft  
Aft Rotor  
Automatic Flight Control System  
Autorotation  
Axis of No Feathering  
Boeing  
Chinook  
Classical Rotor Model  
Collective Pitch  
Differential Airspeed Hold (DASH) System  
Differential Collective pitch Trim (DCPT)  
Equations of Motion  
External Load  
Forward Rotor  
Fuselage  
Gross Weight  
Ground Effect  
Initial Condition (IC)  
Integrated lower Control Actuator (ILCA)  
Lateral Cyclic Pitch  
Longitudinal Cyclic Pitch  
Math Model  
Real Time Task  
RAF HC MK2  
Rotor Model  
Shaft Horsepower  
Shaft Normal Plane  
Simulation Math Model  
Sling Load Model  
Tandem Rotor Helicopter

## TABLE OF CONTENTS

<b>1.</b>	<b>SUMMARY.....</b>	<b>8</b>
<b>2.</b>	<b>INTRODUCTION .....</b>	<b>11</b>
2.1.	Major Model Assumptions .....	11
2.1.1.	Classical Rotor Model .....	11
2.1.2.	Blade Element Rotor Model .....	12
2.1.3.	Fuselage Model.....	12
2.1.4.	Mechanical Control Systems.....	13
2.1.5.	Automatic Flight Control System (AFCS).....	13
2.1.6.	Accessory Losses .....	14
2.1.7.	Time-Dependent Values .....	14
2.1.8.	Trim Tolerances .....	14
2.1.9.	Integration Axes .....	14
2.1.10.	Small Angle Assumptions .....	14
2.1.11.	Landing Gear .....	14
2.2.	Program Architecture.....	14
<b>3.</b>	<b>AIRFRAME .....</b>	<b>15</b>
3.1.	Equations of Motion.....	15
3.1.1.	Basic Airframe Equations Of Motion (EOM) And Euler Angle Rotation .....	17
3.1.2.	Aircraft Body Axis Linear Velocity Resolution .....	20
3.1.2.1.	Total Linear Velocity Summation.....	20
3.1.2.2.	Wind Models .....	21
3.1.2.2.1.	Steady Wind Model .....	21
3.1.2.2.2.	Ramp Wind Model.....	22
3.2.	Classical Rotor Model.....	23
3.2.1.	Linear And Angular Velocities In The Rotor System Leading To Rotor Sideslip Angle ( $\beta'$ ).....	23
3.2.1.1.	Rotor Hub To Shaft Normal Plane Transformation .....	23
3.2.1.2.	S.N.P. to S.N.P. Wind Axis Resolution .....	23
3.2.1.3.	Resolving Body Axis P, Q, and R Into Rotor S.N.P. Wind Axis .....	26
3.2.2.	Rotor Advance And Inflow Ratios, Including Effects Of Rotor/Rotor And Rotor/Fuselage Interference And Inflow Lag .....	27
3.2.2.1.	Rotor Advance Ratio .....	27
3.2.2.2.	Rotor Inflow Ratio ( $\lambda$ ) .....	28
3.2.2.3.	Downwash On Fuselage .....	28
3.2.3.	Rotor Input Collective And Cyclic Pitch Controls ( $\theta_0$ , $B_{1c}$ , $A_{1c}$ ).....	28
3.2.4.	Rotor Flapping Equations.....	29
3.2.4.1.	Assumptions.....	29
3.2.4.2.	Basic Flapping Equations.....	30
3.2.4.3.	Rotor Flap Uncoupling Derivation .....	31
3.2.5.	Rotor Forces And Moments .....	31
3.3.	Blade Element Rotor (BER) Model.....	31
3.3.1.	Introduction to BER Model .....	31
3.3.2.	Coordinate Systems and Transformations .....	32
3.3.2.1.	Body and Hub Axes.....	32
3.3.2.2.	Shaft Axes.....	34
3.3.2.3.	Rotating Shaft Axes.....	34
3.3.2.4.	Blade Element Axes.....	34
3.3.3.	Geometry of Blade Elements .....	35
3.3.3.1.	Rotation Angles .....	35
3.3.3.2.	Element Radial Location .....	35

3.3.4.	Calculation of States Fixed with respect to Rotor .....	36
3.3.4.1.	Translational Velocity .....	36
3.3.4.2.	Translational Acceleration .....	36
3.3.4.3.	Angular Velocity and Acceleration .....	36
3.3.5.	Rotor Inflow Model .....	37
3.3.5.1.	Modified for Ground Effect .....	37
3.3.5.2.	Application of Inflow Lag .....	37
3.3.5.3.	Rotor-on-Rotor Interference .....	37
3.3.6.	Non Uniform Inflow .....	37
3.3.7.	Element Model .....	37
3.3.7.1.	Calculation of States Fixed Along Blade .....	37
3.3.7.2.	Calculation of Velocity Components Fixed Along Blade .....	38
3.3.7.3.	Calculation of Local Element States .....	38
3.3.7.3.1.	Geometric Pitch .....	39
3.3.7.3.2.	Local Segment Velocities .....	39
3.3.7.3.3.	Segment Angle of Attack and Application of Sweep Theory .....	40
3.3.7.4.	Calculation of Element Local Lift and Drag Coefficients .....	42
3.3.7.4.1.	Simplified Model (AERCHAR = 0) .....	42
3.3.7.4.2.	Table Lookup to Determine $C_l$ and $C_d$ (AERCHAR = 2) .....	42
3.3.8.	Calculation and Summation of Blade Angles, Forces and Moments .....	43
3.3.8.1.	Normal, Tangential and Radial Aerodynamic Forces of a Blade Element .....	43
3.3.8.2.	Total Aerodynamic Hinge Moments and Blade Shears in Rotating Shaft Coordinate System .....	43
3.3.8.2.1.	Aerodynamic Flapping and Lagging Moments About Hinge .....	43
3.3.8.2.2.	Aerodynamic Shears .....	43
3.3.8.3.	Flap and Lag Angle Calculation .....	43
3.3.8.3.1.	Flap Angle .....	44
3.3.8.3.2.	Lag Angle .....	44
3.3.8.4.	Inertial Shears, Total Shaft Shears and Total Hub Moments .....	44
3.3.8.4.1.	Calculation of Inertial Shears .....	44
3.3.8.4.2.	Calculation of Total Shaft Shears .....	45
3.3.8.4.3.	Calculation of Total Hub Moments .....	45
3.4.	Fuselage Aero Forces And Moments And Total Force And Moment Summation ....	45
3.4.1.	Determination Of Fuselage Aero Forces And Moments .....	45
3.4.1.1.	Determination of Fuselage Angle of Attack, Sideslip, and Local Dynamic Pressure .....	46
3.4.1.2.	Table Lookup for Fuselage Force and Moment Coefficients .....	47
3.4.1.3.	Equivalent Flat Plate Area ( $\Delta f_e$ ) Corrections .....	48
3.4.1.4.	Wind Tunnel Moment Arm Correction and Calculation of Fuselage Forces and Moments From Coefficients .....	48
3.4.1.5.	Accountability For Rearward Flight .....	49
3.4.2.	Resolution Of Rotor Forces And Moments Into The Aircraft Body Axis And Summation With Fuselage Data .....	49
3.4.2.1.	Moment of Rotor Forces With Resolution of Forces and Moments Into Body Axis .....	49
3.4.2.2.	Summation of Rotor and Fuselage Forces and Moments .....	49
<b>4.</b>	<b>AIRCRAFT DYNAMIC SUBSYSTEMS .....</b>	<b>50</b>
4.1.	Mechanical Controls Model .....	50
4.1.1.	Tandem Rotor Helicopter Flight Controls Scheme .....	50
4.1.2.	Directional Control .....	50
4.1.3.	Roll Control .....	51
4.1.4.	Vertical Control .....	52
4.1.5.	Longitudinal Pitch Control .....	52
4.2.	Automatic Flight Control System (AFCS) Model .....	53
4.3.	Engine Model .....	55

Attachment 1  
8-7430-1-3719

4.3.1. General .....	55
4.3.2. FADEC/55-L-712 Model Operation .....	55
4.4. Rotor Shaft Dynamic System Model.....	56
<b>5. EXTERNAL SLING LOAD.....</b>	<b>56</b>
5.1. General.....	56
5.2. Preliminary Calculations .....	59
<b>6. MODEL VALIDATION DATA .....</b>	<b>59</b>
<b>7. STABILITY DERIVATIVE AND CONTROL SENSITIVITY MODEL OVERVIEW.....</b>	<b>62</b>
<b>8. AIRFRAME TRIM LOOPS.....</b>	<b>62</b>
<b>9. REFERENCES.....</b>	<b>65</b>

## LIST OF FIGURES

FIGURE 1 - CH-47D MATH MODEL STRUCTURE .....	10
FIGURE 2 - HELICOPTER BODY AXIS SYSTEM.....	18
FIGURE 3 - STEADY WIND MODEL $u_w = V_w \cos \theta \cos(\psi - \psi_w)$ .....	21
FIGURE 4 - WIND RAMP VELOCITY .....	22
FIGURE 5 - BODY TO SNP WIND AXIS TRANSFORMATION .....	23
FIGURE 6 - RESOLUTION THROUGH $\beta'$ INTO SNP WIND AXIS .....	24
FIGURE 7 - SKETCH OF SNP WIND AXIS ORIENTATION .....	26
FIGURE 8 - ROTOR BLADE ELEMENT MODEL FLOW DIAGRAM. ....	32
FIGURE 9 - SKETCH SHOWING BODY, HUB AND SHAFT AXES COORDINATE SYSTEMS... 33	
FIGURE 10 - SKETCH SHOWING THE ROTATING SHAFT AXES COORDINATE SYSTEM. ... 34	
FIGURE 11 - SKETCH SHOWING THE BLADE ELEMENT AXES COORDINATE SYSTEM. .... 35	
FIGURE 12 - SKETCH SHOWING BLADE SEGMENT GEOMETRY.....	36
FIGURE 13 - SKETCH SHOWING LOCAL BLADE ELEMENT VELOCITY, ANGLE OF ATTACK AND FORCES. ....	38
FIGURE 14 - SKETCH SHOWING ANGULAR VELOCITY TRANSFORMATION FROM HUB TO HINGE.....	40
FIGURE 15 - SKETCH SHOWING ORIENTATION OF SEGMENT STREAMWISE BLADE PITCH ANGLE. ....	41
FIGURE 16 - RESOLUTION OF LOCAL VELOCITY COMPONENTS INTO THE STREAMWISE BLADE PITCH AXES.....	42
FIGURE 17 - FUSELAGE FORCES AND MOMENTS .....	46
FIGURE 18 - TANDEM ROTOR RESPONSE TO DIRECTIONAL AND LATERAL CONTROL . 51	
FIGURE 19 - TANDEM ROTOR RESPONSE TO COLLECTIVE AND LONGITUDINAL CONTROL .....	53
FIGURE 20 - EXTERNAL LOAD GEOMETRY .....	58
FIGURE 21 - LOAD VELOCITY AND FORCE RESOLUTION .....	59
FIGURE 22 - MATH MODEL TRIM LOOPS .....	64

## LIST OF ABBREVIATIONS AND ACRONYMS

Abbreviation/ Acronym	Definition
AFCS	Automatic Flight Control System
BER	Blade Element Rotor
CG	Center of Gravity
DASH	Differential Airspeed Hold
DF	Rotor on Rotor Interference Factor
EOM	Equations of Motion
FOD	Foreign Object Damage/Debris
ILCA	Integrated Lower Control Actuator
PNF	Plane of No Feathering
OGE	Out of Ground Effect
RPM	Revolutions per Minute
RTT	Real Time Task
SHP	Shaft Horsepower
SNP	Shaft Normal Plane
X	X Force Component
Y	Y Force Component
Z	Z Force Component
L	Rolling Moment
M	Pitching Moment
N	Yawing Moment
P	Roll Rate
Q	Pitch Rate or Torque (depending on situation)
R	Yaw Rate
$\dot{P}$	Roll Acceleration
$\dot{Q}$	Pitch Acceleration
$\dot{R}$	Yaw Acceleration
$\phi$	Roll Attitude
$\theta$	Pitch Attitude
$\psi$	Yaw Attitude
u	X Velocity Component
v	Y Velocity Component
w	Z Velocity Component
$\dot{i}$	

<b>Abbreviation/ Acronym</b>	<b>Definition</b>
$\dot{v}$	X Acceleration Component
$\dot{w}$	Y Acceleration Component
	Z Acceleration Component
T	
H	Rotor Thrust
Y	Rotor H Force
	Rotor Y Force
$\theta_0$	
$B_{1C}$	Collective
	Longitudinal Cyclic
$A_{1C}$	Lateral Cyclic
$a_0$	
$a_1$	Coning
$b_1$	Longitudinal Flapping
	Lateral Flapping
$C_T$	
D	Thrust Coefficient
N	Drag
V	Normal Force
m	Total Speed
g	Mass
q	Gravity
$\alpha$	Dynamic Pressure
$\beta$	Angle of Attack
$\lambda$	Sideslip Angle
$\mu$	Inflow Ratio
$\Omega$	Advance Ratio
$\delta_3$	Rotor Speed
	Delta 3 Hinge Effect Angle
Ixx	
Iyy	Roll Inertia
Izz	Pitch Inertia
Ixy, Iyx, Ixz,	Yaw Inertia
Izx, Iyz, & Izy	Product of Inertia



## 1. SUMMARY

This document presents an overview of the major mathematical calculations and engineering physics used to represent the RAF HC MK2. Explanations and descriptions of the approach used in modeling the rotor, airframe, sling load and aircraft dynamic systems are also included.

The Boeing math model is a total force, full flight envelope, real-time, six-degree-of-freedom, generic tandem rotor helicopter model from which small perturbation stability derivatives may also be obtained. The model utilizes either a simplified classical Fourier approach to rotor modeling or a blade element approach. The simplified classical method was developed by Wheatley and Bailey, which can be found in the public domain. The Boeing math model also has a tandem suspension external sling load capability that couples the load and basic airframe equations of motion.

The program was originally synthesized for the Boeing Vertol 347/HLH control system developmental studies and was mechanized on an AD-4/IBM 360 hybrid analog/digital computer system. The original Boeing Vertol 347 model was later implemented on a  $\Sigma 9$  digital computer in 1974. This initial all-digital programming effort at Boeing was followed by a number of CH-47 aircraft simulation model configuration changes which have been made since then. In the intervening years, the model has also been rehosted to several new computer systems and currently runs on the Silicon Graphics Challenge and Onyx family of computers. The generic model is primarily used for piloted and unpiloted handling qualities and automatic flight controls/stability augmentation system investigations.

The computer math model consists of the following major subsections or divisions:

### Major Model Subsections

- Pre/Post Processing - Precalculated coefficients to save computational time, and a subroutine to zero all computed common variables.
- Standard Mathematical Subroutines - Sine, cosine, trapezoidal integration, fast square root, linear interpolation, etc.
- Equations of Motion - Equations of motion for the aircraft. Sling load calculations are coupled with aircraft equations of motion here.
- Airframe Calculations - Angle of attack and sideslip angles are calculated and used to determine fuselage forces and moments from wind tunnel derived "drag" model data. Classical or blade element rotor modeling approaches

are utilized in evaluating rotor forces, moments and flapping. Rotor on rotor, and rotor on fuselage aerodynamic interference is accounted for, along with corrections to thrust for stall and ground effect. Rotor torque is also corrected for stall and is matched to flight test speed power polar data.

- Control Systems Modeling
  - Mechanical controls
  - AFCS/SAS
  - Engine/governor and rotor shaft dynamics
- Sling Load - Aerodynamic and inertial forces and moment contributions of the sling load.



## 2. INTRODUCTION

### 2.1. Major Model Assumptions

The full flight envelope model is intended for flying qualities studies anywhere within the aircraft flight envelope boundaries; extending from 45 knots rearward flight to  $V_{max}$  forward flight, and from autorotation to max power climb. In the hover/low speed region, sideward velocities up to aircraft limits can be analyzed.

#### 2.1.1. Classical Rotor Model

The classical equation approach to rotor force, moment, and flapping determination is used in the model, and the following assumptions apply to its application:

1. Torque corrections (varying with thrust coefficient,  $C_T$ , and advance ratio,  $\mu$ ) are applied to the output torque, which is later used in moment summation calculations that add rotor and fuselage moments for EOM determination. Rotor thrust limits to account for non-linear rotor lift curve slope (stall effects) are incorporated. Rotor torque is also corrected for stall effects, and then is replaced in the math model by the corrected value.
2. Rotor normal or H force determination is made with a substantially simplified form of the Wheatley-Bailey / Nikolsky approach.
3. Rotor flapping is predicated upon a first harmonic approximation of the Fourier Series expansion for  $a_0$ ,  $a_1$ ,  $b_1$ .
4. Tip loss factor is assumed to be 1.0 (i.e.  $B = 1.0$ ).
5. For rotor-on-rotor interference calculations, 34% overlap wind tunnel derived DF factors are applied in determining  $\lambda$ . Accountability for fuselage sideslip is made in the rotor-on-rotor interference determination.
6. Rotor inflow lag time constant is calculated using a relationship derived from Peters and HaQuang, JAHS 1988, limited between the simulation Nyquist frequency and 2 seconds.
7. Linear blade twist is assumed. No "live twist" due to the tennis racket effect etc., has been incorporated.
8. Constant lift curve slope ( $a$ ) of 5.3 (1/rad) is assumed for rotor force, moment and flapping computations.

9. To calculate fuselage angle of attack, it is assumed that downwash on the fuselage is the undeveloped average rotor induced velocity ( $v$ ). This assumption causes the model to produce less download in hover than the actual aircraft incurs (and hence a lower thrust requirement for both rotors) because downwash at the center line of the rotors approaches ( $3v$ ) on the RAF HC MK2 flight vehicle.
10. Higher order rotor dynamic effects are not modeled and thus high frequency vertical axis response (particularly with a sling load attached) or lateral response associated with coupled lead/lag motion of the rotor blades) is not considered.
11. Delta-three ( $\delta_3$ ) pitch flap coupling capability for both the forward and rear rotors has been incorporated in the model. Control phase considerations associated with  $\delta_3$  have also been included. The RAF HC MK2 Aircraft does not incorporate  $\delta_3$  hinging of either rotor.
12. Rotor calculations are referred to the Shaft Normal Plane (S.N.P.) in the B.H. RAF HC MK2 model. Since the Plane of No Feathering (PNF) control axis is not the reference (as is the case with the Wheatley/Bailey classical equations) additional terms appear in the B.H. rotor model to account for control inputs (cyclic).
13. Ground effect corrections to rotor thrust are made as a function of the ratio of rotor height above ground level to rotor diameter.

#### **2.1.2. Blade Element Rotor Model**

1. Flap and lag hinge locations are assumed to be coincident permitting simplification of the coupling equations for flap, lag, and pitch articulations of the rotor.
2. Rigid blades are assumed; therefore higher order elastic blade modes are not modeled.

#### **2.1.3. Fuselage Model**

1. Fuselage aerodynamic force and moment tables are limited to  $\pm 90^\circ$  for  $\alpha$  and  $\beta$ . The appropriate force and moment signs are changed for rearward flight (i.e. no rearward flight wind tunnel data is used in the model).
2. A  $\Delta$  flat plate drag correction is applied to the fuselage aero forces and moments to account for aircraft components or aerodynamic effects not

present in the wind tunnel test results used in the model. These include the drag of rotor hubs, landing gear, engine screens (either FOD or all-weather), along with interference and momentum drag.

3. Fuselage moment of inertia does not change as a function of payload configuration or fuel distribution etc. in the model data package.

#### **2.1.4. Mechanical Control Systems**

1. Mechanical push rods, bellcranks, walking beams etc. are typically not modeled. The simulation converts inches of cockpit stick travel to equivalent degrees of blade pitch motion at the swashplate. All subsequent calculations after the stick movement use equivalent degrees of blade pitch.
2. Control mixing combines cockpit stick/pedal inputs with AFCS outputs which are then sent to the swashplate to provide either lateral cyclic or collective pitch commands to the rotor model. Total upper boost control input/output limits are modeled.

#### **2.1.5. Automatic Flight Control System (AFCS)**

1. AFCS outputs are modeled with the proper limits incorporated, in addition to the dynamic transfer function nodes such as lags, lead/lag, washouts etc. No higher order AFCS actuator dynamics or frequency modeling is done, since the actuator frequency of the integrated lower control actuator (ILCA) is much higher than would be permitted given the computational time frame. The frequency response model for the ILCA is an empirical model intended to lump the dynamic response of both ILCA and upper boost actuators. Therefore, these transfer functions cannot be used to model the ILCA actuators for other applications.
2. A dual channel AFCS model has been compiled using identical inputs for each channel. If execution-timing constraints do not allow a full two-channel AFCS model, the second channel can be eliminated by replicating the output of the first.

3. The analog hardware of the AFCS is implemented using discrete time elements for each individual dynamic component (i.e. integrator) in the system as opposed to a discrete time equivalent filter for end-to-end transfer functions. The simulation time frame is assumed to be sufficiently short enough in duration to avoid any anomalies that could arise from this approach to discrete time computation of the analog system.

#### **2.1.6. Accessory Losses**

A constant 290 horsepower accessory power loss is assumed for all flight conditions. The losses account for transmission/power train, electrical, and hydraulic power losses.

#### **2.1.7. Time-Dependent Values**

Last time-frame values are used in some calculations if that parameter is needed in an equation before the "new value" has been computed.

#### **2.1.8. Trim Tolerances**

The RAF HC MK2 model is assumed to have "trimmed" at a steady state condition when the time rate of change for all seven values of  $u$ ,  $v$ ,  $w$ ,  $p$ ,  $q$ ,  $r$  and  $h$  are less than 0.001 if the classical rotor model is used and 0.005 if the blade element rotor model is used. The error (change from the previous time step) for each of the above parameters must also be less than 0.001 and 0.005 for the classical and blade element rotor models, respectively. The units of translational parameters are ft/sec, while the rotational parameters are in radians/sec.

#### **2.1.9. Integration Axes**

Integration of accelerations (linear and angular) are done in the body axis of the A/C and then transformed into the inertial axes as required.

#### **2.1.10. Small Angle Assumptions**

Small angle assumptions are used in the derivation of some equations where applicable (i.e. if  $\beta$  is sufficiently small, then  $\cos \beta = 1$ ,  $\sin \beta = \beta$  etc.).

#### **2.1.11. Landing Gear**

Landing gear equations are not included in the airframe model, but are a separate subroutine which may be exercised if desired (no description of the landing gear model is included in this report).

### **2.2. Program Architecture**

The math model consists of two major subsections, along with appropriate input/output interfacing to facilitate its use. These major program subsections include:

1. Airframe - which covers the calculation of all major fuselage and rotor forces and moments, and the rigid body equations of motion that describe flight dynamics. Airframe computations are modeled with FORTRAN coding.
2. Aircraft Dynamic Subsystems - which include the mechanical and automatic flight control systems, and the engines and rotor shaft dynamic systems, are modeled using C code generated by VISVEC, the Boeing digital modeling tool used to represent dynamic system elements (as one would represent them with an analog computer).
3. Model I/O - which includes a special interfacing subroutine that calculates input variables used more than once in the model, before the real time task (RTT) is executed. Another subroutine executed at the start of the RTT accounts for environmental considerations such as steady or dynamic wind components impinging on the airframe. Output interface routines include the capability for "dumping" analog system output parameters onto tape or individual brush recorder channels, or trim information in tabular "trim sheet" format on a line printer.

### **3. AIRFRAME**

The airframe dynamic model utilized for the RAF HC MK2 full-force tandem helicopter simulation is described in this section. For the purpose of this description, airframe computations include the rigid body equations of motion, rotor system force and moment calculations, fuselage aerodynamic assessment and the final summation of all fuselage and rotor terms. Other aircraft elements including the mechanical and automatic control systems, engine and rotor shaft dynamic systems, and the external sling load model are discussed in subsequent sections.

#### **3.1. Equations of Motion**

Calculations performed in this math model are mechanized in a sequential order intended to maximize calculation speed and at the same time suppress any tendency toward undesirable digital effects. While the computational order may be best from a modeling standpoint, it leads nevertheless to difficulty in describing the physics of what is actually being simulated. Most calculations are described in the order in which they are performed, but when they are covered in a different sequence, appropriate annotations are made in the text.

The classical and blade element rotor (BER) models are described in subsequent subsections. Although the BER model is the default (NROTOR=4), an option to run a "classical" rotor model exists (NROTOR=1). Both the BER and the classical rotor models use the same rigid body equations of motion and force and moment summation equations. A brief outline of the airframe model with the classical rotor model follows:



### Airframe Calculation Summary (Classical Rotor Model)

1. Rigid body equations of motion (including sling load effects) are solved, providing linear and angular accelerations about all three body axes of the aircraft. Euler angle rotations are performed to orient the aircraft in inertial space. Roll acceleration ( $\dot{P}$ ) has been uncoupled from yaw acceleration ( $\dot{R}$ ), to facilitate digital computation.
2. Total linear velocity components in the aircraft body axis are derived by summing aircraft inertial velocities (calculated by integrating the accelerations from the equations of motion) with steady wind components and ramp wind components.
3. Remote total velocity is resolved through the rotor shaft incidence angle (and this is then corrected for aircraft pitching motion) to derive rotor shaft normal plane (S.N.P.) wind axis velocities, and local rotor sideslip values for each rotor ( $\beta'$ ).
4. Individual rotor advance ratios ( $\mu$ ) and inflow ratios ( $\lambda$ ) are computed. Inflow ratio calculations include accountability for rotor-on-rotor aerodynamic interference. Separate calculations determine rotor-on-fuselage downwash interference levels for later use in defining fuselage angle of attack.
5. Rotor input collective and cyclic pitch controls ( $\theta_0$ ,  $B_{1C}$ , and  $A_{1C}$ ) are compiled from the mechanical and automatic flight control system outputs. Both longitudinal and lateral cyclic controls are resolved through the control phase angle ( $\phi_p$ ), and rotor sideslip angle ( $\beta'$ ), to align rotor control inputs orthogonal to the local wind. Forward and aft rotor cyclic pitch inputs are then corrected for delta-three ( $\delta_3$ ) hinging effects (if the aircraft is configured with either forward or aft rotor  $\delta_3$  hinging). Note that the RAF HC MK2 aircraft does not utilize  $\delta_3$  hinges.
6. Coning ( $a_0$ ), longitudinal ( $a_1$ ), and lateral ( $b_1$ ) first harmonic Fourier flapping coefficients are computed using simple "classical" (Wheatley-Bailey) rotor equations. The rotor control inputs and the three flap angle expressions have been rearranged for simultaneous solution, to ensure a digital result which is not based upon data from the previous time frame.

7. Rotor forces and moments are computed using the simple classical equation approach. Forces and moments are computed initially in an axis system oriented perpendicular and parallel to the shaft normal plane, and aligned with the local wind (S.N.P. wind axis).
8. Fuselage total linear velocity components are computed using a vertical velocity term ( $W_T'$ ) that accounts for the rotor on fuselage downwash component described in 4 above. Local angle of attack ( $\alpha_{FUS}$ ) and sideslip ( $\beta_{FUS}$ ) values are derived from these total velocity components. Using the  $\alpha$  and  $\beta$  arguments, fuselage aerodynamic force and moment coefficients are calculated from tabular wind tunnel derived (body-axis) data. The coefficient data are then multiplied by local fuselage dynamic pressure "q" (which includes rotor downwash) to produce final force and moment results.
9. Rotor aerodynamic forces and moments (applied at the hub) are resolved through the rotor sideslip and shaft incidence angles back into the aircraft body axis. Summation of these rotor forces and moments with the fuselage body axis force and moment results is performed. Moments generated by imposition of individual rotor forces on the airframe are computed next and added into the overall moment summation. The resulting rotor and fuselage force and moment totals are finally inserted into the equations of motion to again compute the airframe acceleration set.
10. When external sling load computations are performed, the EOM set is modified to account for the effects of load-induced forces and moments imposed upon the airframe. Sling load sway angle accelerations and velocities (which consider load aerodynamic effects calculated just before the moment summation described in 9 above) are first calculated separately, and then are utilized to compute the airframe EOM set.

### **3.1.1. Basic Airframe Equations Of Motion (EOM) And Euler Angle Rotation**

The helicopter is modeled as a rigid body, with symmetry assumed about the X-Z plane so that the  $I_{XY}$  and  $I_{YZ}$  product of inertia terms are zero. Linear and angular accelerations of the airframe are expressed in the helicopter body axis system depicted in Figure 2. Positive axis directions are annotated with large arrowheads. Positive accelerations and velocities are coincident with the directions of the axes. As indicated earlier, the X, Y, and Z forces and L, M, and N moments contain only aerodynamic terms.

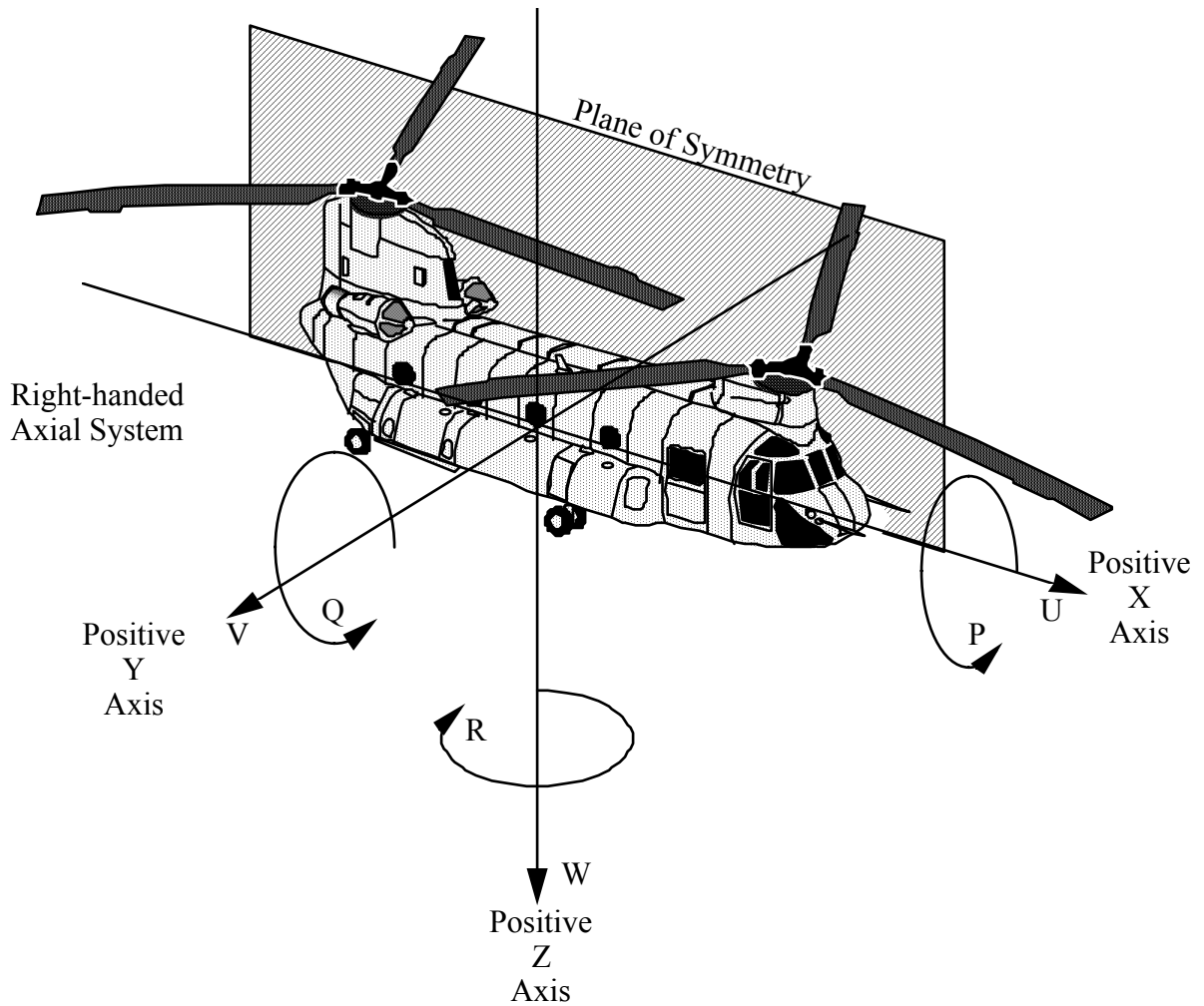


Figure 2 - Helicopter Body Axis System

In order to keep the explanation of the equations of motion (EOM) as simple as possible, terms associated with external sling load dynamics have been removed from the initial set of EOM expressions presented. These additional sling load terms and calculations will be discussed in Section 5.

The basic airframe rigid body equations of motion are straight forward, and may be found in several reference texts describing aircraft flight dynamics (i.e., Etkin's "Dynamics of Atmospheric Flight", Page 149 and Thelander's "Aircraft Motion" analysis, Page 65; (References 3 and 4). These equations are presented below:

Equations of Motion - Linear Acceleration

$$\dot{u} = \frac{X}{m} - g \sin \theta + Rv - Qw \quad (3.1)$$

$$\dot{v} = \frac{Y}{m} + g \sin \phi \cos \theta + Pw - Ru \quad (3.2)$$

$$\dot{w} = \frac{Z}{m} + g \cos \phi \cos \theta + Qu - Pv \quad (3.3)$$

### Angular Acceleration

$$\dot{P} = \frac{L}{I_{xx}} + \left( \frac{I_{xz}}{I_{xx}} \right) (\dot{R} + PQ) + \left[ \frac{(I_{yy} - I_{zz})}{I_{xx}} \right] QR \quad (3.4)$$

$$\dot{Q} = \frac{M}{I_{yy}} + \left( \frac{I_{xz}}{I_{yy}} \right) (R^2 - P^2) + \left[ \frac{(I_{zz} - I_{xx})}{I_{yy}} \right] PR \quad (3.5)$$

$$\dot{R} = \frac{N}{I_{zz}} + \left( \frac{I_{xz}}{I_{zz}} \right) (\dot{P} - QR) + \left[ \frac{(I_{xx} - I_{yy})}{I_{zz}} \right] PQ \quad (3.6)$$

Since the  $\dot{R}$  equation follows the  $\dot{P}$  expression in the program, the current value of  $\dot{P}$  is available for use in the  $\dot{R}$  equation. It should also be noted that P, Q, R,  $\theta$ ,  $\phi$ , X, Y, Z, L, M, N are values computed in the previous time frame. **Note:** To reduce computational time, slingload coefficients have been synthesized from combinations of slingload physical parameters such as mass, cable length cable separation, inertias, etc., as discussed in Section 5.

After computation, the linear and angular accelerations presented above are then integrated with respect to time to obtain the aircraft body axis linear and angular velocities.

$$u = \int \dot{u} dt \quad (3.7)$$

$$v = \int \dot{v} dt \quad (3.8)$$

$$w = \int \dot{w} dt \quad (3.9)$$

$$P = \int \dot{P} dt \quad (3.10)$$

$$Q = \int \dot{Q} dt \quad (3.11)$$

$$R = \int \dot{R} dt \quad (3.12)$$

The linear body axis velocities u, v, w obtained in equations 3.7, 3.8 and 3.9 are now resolved through the  $\theta$  (pitch), and  $\phi$  (roll) angles down onto the earth plane (i.e., a plane tangent to the earth's surface below the aircraft CG) to produce  $X_E$ ,  $Y_E$  and  $Z_E$  (where  $Z_E$  is equivalent to  $-H_E$ ). Note:  $H_E$  is positive up. These

Earth velocities are typical of what would be produced by a carousel inertial navigation system and are sometimes used in AFCS modeling.

The earth axis velocities may now be used to compute the inertial axis velocities by rotating through  $\psi$  to obtain  $X_I$ ,  $Y_I$ , and  $H_I$  (note that  $-Z_E = H_E = H_I$  which is positive in an upward direction).  $X_I$ ,  $Y_I$  and  $H_I$  represent the North/South, East/West and upward linear velocities of the aircraft CG respectively. These parameters may be used by an Inertial Measuring Unit (IMU) on the aircraft (not implemented in the RAF HC MK2 math model) or for the drive arguments associated with an optical probe or CGI type simulation visual display.

Earth or Inertial axis velocities may then be integrated in the same manner as the body axis velocities to obtain X, Y, and Z displacement information. These integrated displacement values may be used for control systems, Distance Measuring Equipment (DME), optical probe limits (for a terrain board type visual display) etc.

The Euler rotation angles  $\psi$ ,  $\theta$ , and  $\phi$  represent the previous time frame values of yaw, pitch, and roll angle, and orient the helicopter airframe in the inertial coordinate system. Note:  $\phi$ ,  $\theta$ ,  $\psi$ , P, Q and R are values obtained from the last time frame calculations.

Sling load equations of motion, and their various contributions to the aircraft acceleration set (including suspension sway angle accelerations, velocities and angles) are also calculated in this section of the program. Description of the sway angle equations is deferred until Section 5.

Computations associated with the Automatic Flight Control System (AFCS), engine and rotor shaft dynamic system, and the mechanical controls are carried out immediately after the Euler integrations described above. As indicated earlier, discussion of these dynamic elements are deferred until later in order to maintain continuity in describing model physics. The aircraft body axis linear velocity resolution will be discussed next.

### **3.1.2. Aircraft Body Axis Linear Velocity Resolution**

#### **3.1.2.1. Total Linear Velocity Summation**

In order to compute the fuselage aerodynamic forces and moments, the rotor sideslip ( $\beta'$ ) angles, inflow ratios ( $\lambda$ ), or advance ratios ( $\mu$ ), it is first necessary to calculate the total velocities acting on the fuselage and rotor systems. Total velocity includes the inertial u, v, and w components along with steady and variable wind components. The wind representations programmed in the Boeing tandem rotor simulation include steady and ramp gust models. After the selected wind (or winds) are calculated and resolved into the body axis of the aircraft, the total resultant velocities are obtained:

$$u_T = u + u_w + u_r \quad (3.13)$$

$$v_T = v + v_w + v_r \quad (3.14)$$

$$w_T = w + w_w + w_r \quad (3.15)$$

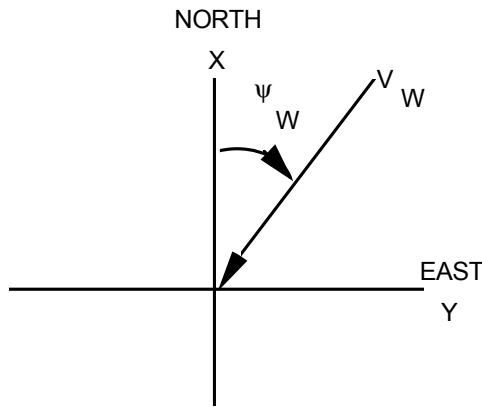
Total aerodynamic velocity in body axis used for defining $\alpha$ & $\beta$	A/C Inertial Velocity (Body axis ground speed) as defined by equations 3.7 to 3.9	Steady wind velocity resolved into a/c body axis	Ramped wind velocity resolved into a/c body axis
--	---	--	--

The steady wind models, as discussed next, are programmed directly after the EOM calculations.

### 3.1.2.2. Wind Models

#### 3.1.2.2.1. Steady Wind Model

"Steady" wind velocities introduced above are based upon a steady wind ( $V_w$ ) blowing from a fixed azimuth ( $\psi_w$ ) in the inertial X-Y plane onto the helicopter. Wind velocity  $V_w$  does not have an upward component. Resolution of this wind from the fixed inertial axis into the aircraft body axis (and rotor axes, as will be explained later) is accomplished as follows:



$$u_w = V_w \cos \theta \cos(\psi - \psi_w) \quad (3.16)$$

$$(3.16)$$

$$v_w = V_w [\sin \theta \sin \phi \cos(\psi - \psi_w) - \cos \phi \sin(\psi - \psi_w)] \quad (3.17)$$

$$(3.17)$$

$$w_w = V_w [\sin \theta \cos \phi \cos(\psi - \psi_w) + \sin \phi \sin(\psi - \psi_w)] \quad (3.18)$$

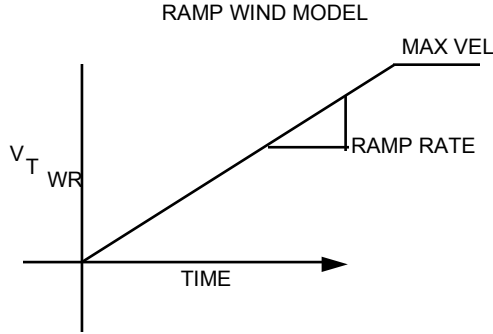
$$(3.18)$$

Figure 3 - Steady Wind Model

where:  $V_w$  = total steady wind velocity  $\psi_w$  = direction from which wind blows expressed from 0 to  $\pm 180^\circ$   $u_w, v_w, w_w$  are components of steady wind along aircraft X, Y, and Z axes respectively.

### 3.1.2.2.2. Ramp Wind Model

The wind ramp model represents a steadily increasing (or decreasing) wind velocity with time. Velocity changes cease when maximum selected values are reached.



$$V_{TWR} = V_{TWROLD} + V_{TWRRATE} \Delta t \quad (3.19)$$

Figure 4 - Wind Ramp Velocity

If the wind ramp velocity ( $V_{TWR}$ ), shown in Figure 4 becomes greater than the maximum velocity selected ( $V_{TWRMAX}$ ), then the total velocity ( $V_{TWR}$ ) is fixed at the maximum value selected.

Since the ramp wind is similar to the steady state wind model, the wind direction diagram shown in Figure 3 is still applicable. Thus the transformation into the aircraft body axis is identical to that of the steady state model as shown below:

$$U_R = V_{TWR} \cos \theta \cos(\psi - \psi_w) \quad (3.20)$$

$$V_{WR} = V_{TWR} [\sin \theta \sin \phi \cos(\psi - \psi_w) - \cos \phi \sin(\psi - \psi_w)] \quad (3.21)$$

$$W_{WR} = V_{TWR} [\cos \phi \sin \theta \cos(\psi - \psi_w) + \sin \phi \sin(\psi - \psi_w)] \quad (3.22)$$

Where:  $U_{WR}, V_{WR}, W_{WR}$  are the components of the ramp wind along the X, Y, and Z axis respectively.  $\theta, \phi, \psi$  are the aircraft Euler angles.

### 3.2. Classical Rotor Model

#### 3.2.1. Linear And Angular Velocities In The Rotor System Leading To Rotor Sideslip Angle ( $\beta'$ )

Rotor forces, moments, and flapping can be calculated as soon as the individual control inputs, local sideslip values, and inflow and advance ratios are known. Rotor calculations are initiated by first determining local sideslip angle ( $\beta'$ ). This is accomplished by summing the total airframe linear velocity components with the tangential velocity at each rotor (relative to the aircraft C.G.) caused by aircraft pitch, roll and yaw motion.

##### 3.2.1.1. Rotor Hub To Shaft Normal Plane Transformation

Linear velocities at each rotor hub are next resolved through the shaft incidence angles ( $i_F, i_R$ ) into the shaft normal plane (S.N.P.), as shown below in Figure 5 for both the forward and aft rotors.

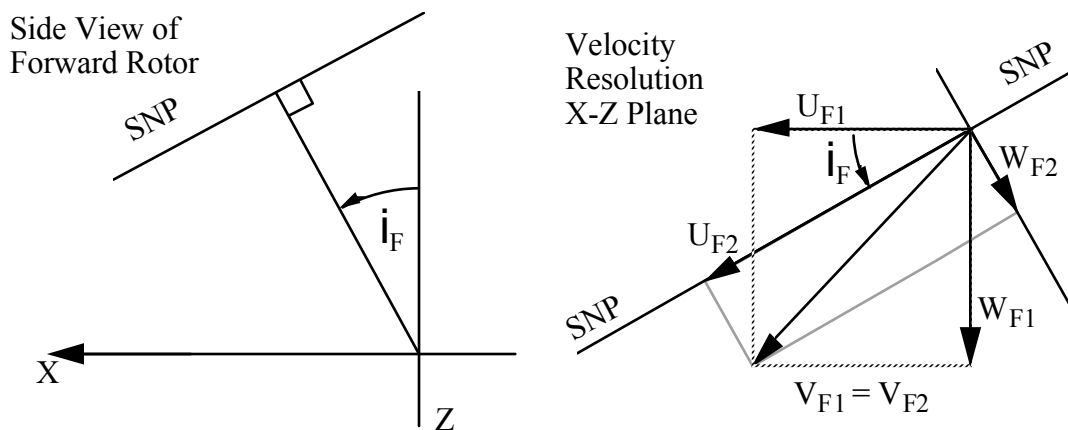


Figure 5 - Body to SNP Wind Axis Transformation

##### 3.2.1.2. S.N.P. to S.N.P. Wind Axis Resolution

According to classical rotor theory, all rotor force, moment, and flapping calculations are based upon the assumption that the rotor faces directly into the wind with no sideward velocity present. In order to meet this requirement for no sideward velocity,  $u_{F2}$  and  $v_{F2}$  (along with  $u_{R2}$  and  $v_{R2}$ ) are resolved through the appropriate rotor sideslip angle ( $\beta'_F$  or  $\beta'_R$ ) into the "S.N.P. Wind Axis". A single velocity vector in the rotor S.N.P. is formed and is defined as being parallel to the local wind direction. This vector is called  $u_F$  (or  $u_R$  for the aft rotor).

Figure 6 below shows how  $u_F$  and  $u_R$  are defined with respect to the X and Y axes of the rotor (or body).



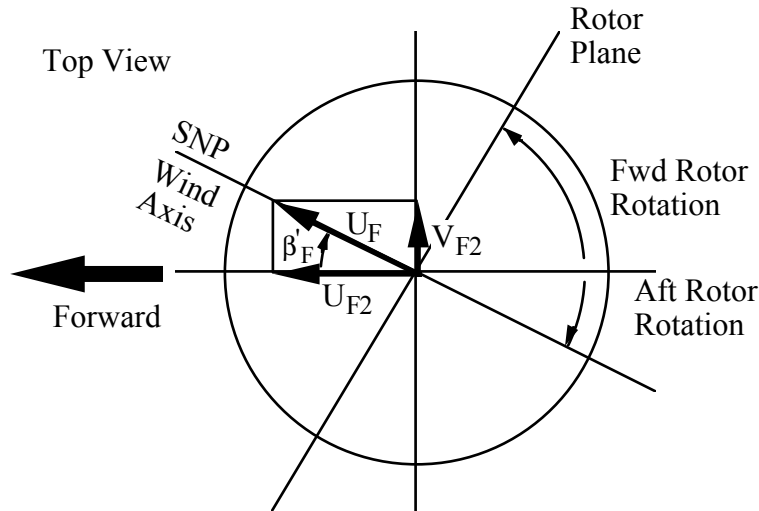


Figure 6 - Resolution Through  $\beta'$  into SNP Wind Axis

Note that  $u_F$  and  $u_R$  will always have positive signs, resulting in only positive values for rotor advance ratio ( $\mu$ ), as will be shown later.

Rotor sideslip angle is used extensively in resolving forces and moments calculated in the rotor S.N.P. wind axis back into an axis system perpendicular and parallel to the aircraft body axis. This rotor sideslip angle is determined as follows:

Forward Rotor

$$\beta'_F = \tan^{-1} \frac{V_{F2}}{u_{F2}} \quad (3.23)$$

Rear Rotor

$$\beta'_R = \tan^{-1} \frac{V_{R2}}{u_{R2}} \quad (3.24)$$

Sine and cosine values are determined after  $\beta'_F$  and  $\beta'_R$  are calculated.

Along with  $u_F$  and  $u_R$  defined above, another velocity perpendicular to the S.N.P. is defined:

$$w_F = w_{F2} \quad (3.25)$$

and

$$w_R = w_{R2} \quad (3.26)$$

These are utilized in computing the component of rotor inflow ratio resulting from the free stream velocity ( $\lambda'$ ). Lamda prime is analogous to the  $V \sin\alpha_{\text{SHAFT}}$  term often used in classical rotor inflow theory derivations, where:

$$\lambda = \frac{V \sin\alpha_{\text{SHAFT}}}{\Omega R} - \frac{v}{\Omega R} \quad (3.27)$$

Where:

$V$  = Total free stream velocity  
 $v$  = rotor induced velocity

In addition to being used in individual rotor inflow computations,  $w_F$  and  $w_R$  are also found in rotor-on-fuselage interference terms.

A comprehensive picture of S.N.P. wind axis orientations with both rotors installed on the helicopter is given in Figure 7. In this diagram, the relationships between the rotor incidence and sideslip angles, linear velocities, and principal forces and moments in the rotor system are delineated. Direction of the arrowhead shows positive direction for the particular parameter.

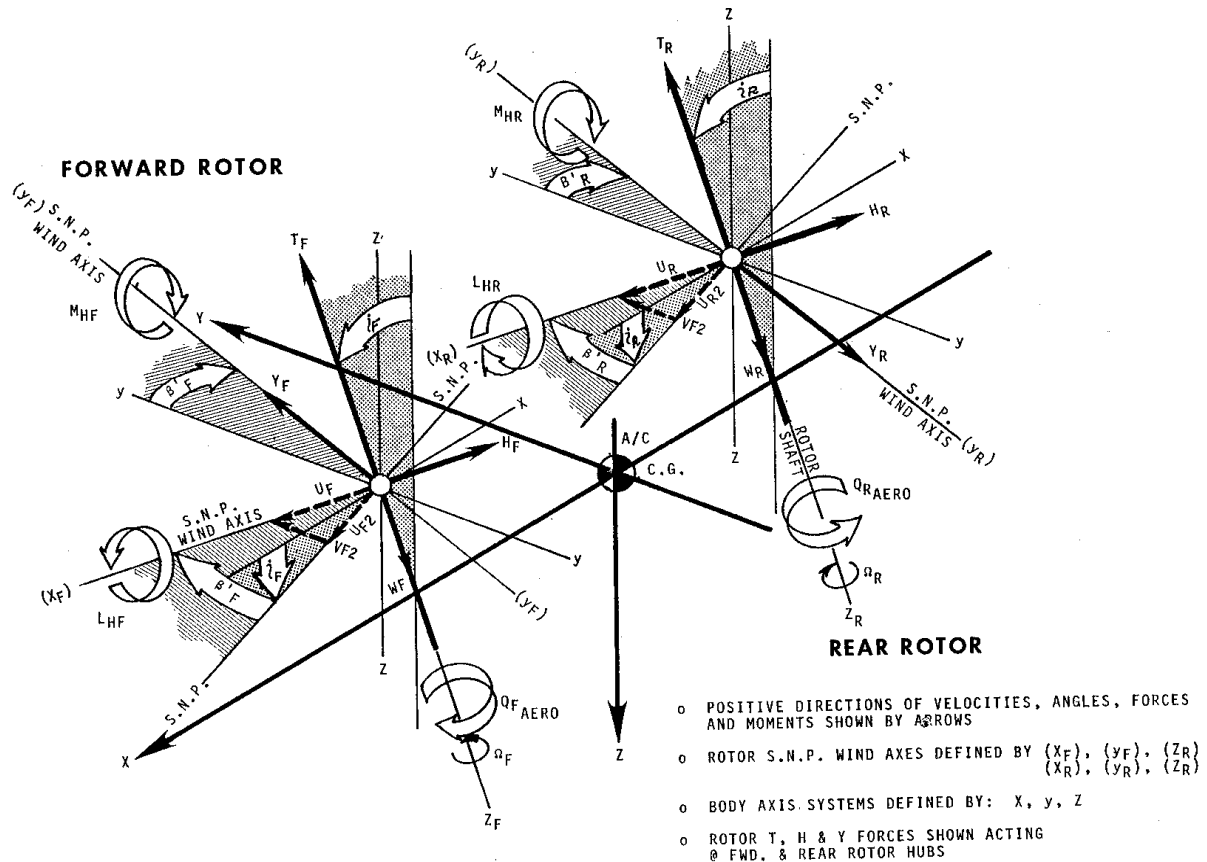


Figure 7 - Sketch of SNP Wind Axis Orientation

### 3.2.1.3. Resolving Body Axis P, Q, and R Into Rotor S.N.P. Wind Axis

When the shaft of a helicopter rotor is subjected to either pitch, roll, or yaw motion, the rotor disc plane lags behind the movement of the shaft because of aerodynamic damping. The magnitude of this lag (in radians) is proportional to the product of the angular pitching (or rolling) rate, and the well known  $16/\gamma\Omega$  (Locke number associated) rotor flapping time constant. This  $P(16/\gamma\Omega)$  or  $Q(16/\gamma\Omega)$  damping parameter is used to correct calculated quasi-static longitudinal ( $a_1$ ) and lateral ( $b_1$ ) rotor flapping for the effects of airframe angular rates.

Since classical calculations for rotor flapping assume that the rotor faces into the wind, angular rates in the rotor system must also be aligned parallel and perpendicular to the local wind vector, before computed flap angles can be corrected for aerodynamic damping. This alignment is achieved by resolving the body axis P, Q, and R angular rates through the shaft incidence and local rotor sideslip angles into the S.N.P. wind axis.

In addition to airframe pitch and roll rate resolution into the S.N.P. wind axis, yaw rate must also be resolved into this axis to permit calculation of the absolute rotational speed for each rotor. Rotor shaft speed ( $\Omega$ ) has to be corrected for

airframe angular rotational rate, in order to produce the actual rotational velocity of the rotor in inertial space. This inertial  $\Omega$  is used in all rotor force, moment and flapping calculations performed in the math model. The signs on  $P_R$  and  $R_R$  are reversed to account for clockwise rotation, since classical rotor equations are derived for counter clockwise rotation.

### 3.2.2. Rotor Advance And Inflow Ratios, Including Effects Of Rotor/Rotor And Rotor/Fuselage Interference And Inflow Lag

Rotor advance and inflow ratios ( $\mu$  and  $\lambda$ ) are defined as the ratio of the rotor S.N.P. wind axis longitudinal and vertical velocity components, respectively, to the rotor tip speed.

#### 3.2.2.1. Rotor Advance Ratio

Advance ratio is defined as the non-dimensional free stream velocity parallel to the S.N.P., divided by the rotor tip speed.

$$\frac{V \cos \alpha_{\text{SHAFT}}}{\Omega R_B}$$

Since the simulation model is based on S.N.P. resolution of rotor variables, advance ratio ( $\mu$ ) is calculated in the following manner:

#### FORWARD ROTOR

$$\mu_F = \frac{u_F}{R_B \Omega_F} = \frac{u_F}{V_{\text{TIP}_F}} \quad (3.28)$$

Where:  $u_F$  is the longitudinal velocity component in the S.N.P. wind axis.  $\Omega_F$  is the inertial rotational speed of the forward rotor described below, and  $R_B$  is the forward rotor radius.

In this advance ratio calculation,  $\Omega_F$  is determined by adding the rotational speed of the rotor shaft caused by the engines and rotor dynamic system (and computed in the Rotor Shaft Dynamic Model) to the rotational speed of the rotor caused by airframe angular motion.

$$\Omega_F = \Omega'_F - R_F \quad (3.29)$$

Rotor speed in inertial reference system	=	Rotor shaft rotational speed W.R.T. the fuselage - (from Engine/Shaft Dynamic Model)	-	Airframe yaw angular rotation referred to SNP wind axis
---	---	---	---	--

also:

$$V_{TIP_F} = R_B \Omega_F \quad (3.30)$$

### REAR ROTOR

$$\mu_R = \frac{u_R}{R_B \Omega_R} = \frac{u_R}{V_{TIP_R}} \quad (3.31)$$

#### **3.2.2.2. Rotor Inflow Ratio ( $\lambda$ )**

Rotor inflow ratio is comprised of a series of terms arising from the free stream velocity passing through the rotor (perpendicular to the S.N.P.) and from the following rotor induced flow components: free stream component, induced velocity component, and other rotor interference component.

#### **3.2.2.3. Downwash On Fuselage**

Before leaving the discussion of rotor inflow, it is noted that forward rotor  $\lambda_3$  (the total induced flow with aft rotor interference and inflow lag corrections applied) is used to approximate rotor downwash on the fuselage for angle of attack calculations. In the derivation of rotor on fuselage interference velocity, it is assumed that the average induced velocity of the forward and aft rotor acts on the fuselage to modify the angle of attack caused by free stream flow.

It is further assumed that the induced flow seen by the fuselage is "undeveloped" (i.e. not contracted), or equivalent to (1 times  $v$ ) at the rotor discs. This assumption leads to reduced fuselage download in hover, but is closer to being correct in forward flight.

#### **3.2.3. Rotor Input Collective And Cyclic Pitch Controls ( $\theta_0$ , $B_{1c}$ , $A_{1c}$ )**

As indicated earlier, the physical modeling of the RAF HC MK2 flight control system is not dealt with in this section of the report. This section covers instead the special treatment of collective and cyclic control input, which is a prerequisite for using this control information to compute rotor forces, moments, or flapping.

Regardless of whether the pilot or the automatic flight-control system (AFCS) introduces the control, each rotor of a tandem helicopter ultimately sees only three types of input. They are:

1. Collective Pitch ( $\theta_0$ ) Caused by longitudinal stick or AFCS motion which produces differential collective pitch (DCP), or collective stick which produces collective pitch at the rotors.

2. Longitudinal Cyclic ( $B_{1c}$ ) Resulting from airspeed derived dynamic pressure sensed cyclic trim. This is the only longitudinal cyclic pitch (LCP) control currently available on all of the CH-47D aircraft, but "cyclic on the stick" type inputs may be generated through the AFCS (or cockpit input) to enhance low speed longitudinal maneuverability.
3. Lateral Cyclic ( $A_{1c}$ ) Produced by a combination of lateral stick and pedal or AFCS type inputs.

Cyclic pitch is the more complex of these control inputs as far as "preprocessing" prior to use in the classical equations is concerned.

### **3.2.4. Rotor Flapping Equations**

#### **3.2.4.1. Assumptions**

Representation of rotor flapping in the Boeing rotor model is accomplished with quasi-steady state Wheatley/Bailey "classical" equations. The final simplified classical flapping expressions are based upon the following assumptions:

1. First harmonic theory (i.e. flapping may be described by the first 3 terms of a Fourier series).
2. Uniform inflow (downwash does not vary as a function of rotor radius) - constant over the entire rotor.
3. No reverse-flow effects.
4. Uniformly twisted, untapered blades.
5. Rigid blades.
6. Negligible hinge offset.
7. Zero tip-loss factor.
8. No delta-three pitch-flap coupling effects are incorporated in the force, moment and flapping equations (these are accounted for by correcting input controls as discussed earlier). Decoupling between control inputs (which depend upon flap angles), and flap angles which depend upon the controls, has been accomplished to facilitate digital computation.
9. Limited treatment of rotor compressibility and stall effects is included - "Stall  $C_T/\sigma$  limits and torque  $\Delta Q$  corrections" are applied to thrust and torque after they are computed from classical equations.

10. Lift slope is constant and drag coefficient varies only with  $C_L$ . A correction to account for the rotor  $C_T/\sigma$  lift curve slope decrease associated with rotor stall is contained within an optional subroutine called "RSTALL".
11. Forward and rear rotor equations have identical form.

These assumptions are also applicable to the classical rotor forces and moments.

#### **3.2.4.2. Basic Flapping Equations**

Expressions describing rotor blade flapping motion may be obtained by equating the moments of rotor thrust and centrifugal force about the flapping hinge to zero (Reference 1 p. 153). This flapping motion can be described as an infinite Fourier series expansion, written as a function of blade position around the azimuthal path, with coefficients defined relative to the aircraft longitudinal and lateral axis.

Only the 1st harmonic of this flapping expansion needs to be determined, since the remaining terms are of the same order of magnitude as the elastic blade deflections (which were neglected in the derivation of the classical equations and assumption number 5). The first three terms of the expansion  $a_0$ ,  $a_1$ , and  $b_1$  represent in the physical world the coning, longitudinal and lateral flapping of the rotor system.

It should be noted that the rear rotor equations are identical in form to the forward rotor equations except for the direction of rotation of the rotor being considered.

As was discussed earlier, when the helicopter rotor shaft is subjected to an aircraft pitching or rolling motion, the rotor disc plane response tends to lag behind the shaft movement because of aerodynamic damping. The magnitude of this damping term, which is expressed as a flapping lag (in radians) behind the shaft tilt, is inversely proportional to Locke number and rotor speed. It varies directly with the square of advance ratio and the product of either the roll or pitch rate of the aircraft.

A dynamic flap response lag of the rotor system is implicit in the model, because of the manner in which the flight control inputs and flapping calculations are ordered. The one time frame modeling transport delay between control input and calculation of flap response causes a flapping response lag.

The flapping equations are dependent on the controls. As indicated before, the controls are also a function of the flapping when delta-three hinging is used. This, in effect, makes the flapping results dependent upon the flap angles because of the control coupling. It is therefore necessary to uncouple the flapping equations so that they are only a function of the controls (before they are corrected for delta-three effects).

#### **3.2.4.3. Rotor Flap Uncoupling Derivation**

Since the equations just described for flapping depend upon control inputs that vary with flap angle, they must be uncoupled mathematically for digital computation (to avoid using flapping information calculated during the previous time frame). Rotor thrust coefficient ( $C_T$ ), which appears in the coning equation, is also dependent upon the rotor collective and cyclic controls. Thus the rotor thrust expression must be accounted for in the flap uncoupling derivation, along with the delta-three corrected rotor controls. With flap angles and control inputs defined, the six rotor force and moments can be determined. Thrust, normal force, side force, torque and the rolling and pitching moments are discussed next.

#### **3.2.5. Rotor Forces And Moments**

Sign conventions for the principal forces and moments are illustrated in Figure 7. Rotor thrust, normal force, side force, and torque are computed initially as nondimensional coefficients in the form  $2(x)/a\sigma$ , where  $x$  is a coefficient. Alternatively, hub pitching and rolling moments ( $M_{HF}$  and  $L_{HF}$ ) are calculated initially in engineering units (foot pounds). The rotor hub moments are not expressed in coefficient form, but are calculated directly as moments. Except for thrust and torque, all rotor forces and moments computed in the model are utilized in an uncorrected state. To improve simulation fidelity, rotor thrust has a stall-associated correction applied, along with ground effect augmentation which varies with rotor height. Calculated rotor torque is also modified for rotor stall effects.

Discussion of the fuselage aerodynamic forces and moments programmed in the Boeing RAF HC MK2 simulation math model is presented in Section 3.4. With all fuselage and rotor forces and moments determined, summation and transformation of these parameters is carried out in preparation to solving the E.O.M. These final airframe computations are also described in Section 3.4.

### **3.3. Blade Element Rotor (BER) Model**

#### **3.3.1. Introduction to BER Model**

The blade element rotor (BER) model used in BHSim to calculate rotor forces and moments was adapted from the model used in the NASA GenHel helicopter simulation program. This model has been significantly restructured to accommodate a wide variety of requirements such as the ability to model both single and tandem rotors, application of various integration schemes, etc. This description of the blade element model follows the flow and structure of the



FORTRAN code wherever possible. Figure 8 presents a flowchart showing basic overall structure of the BER model.

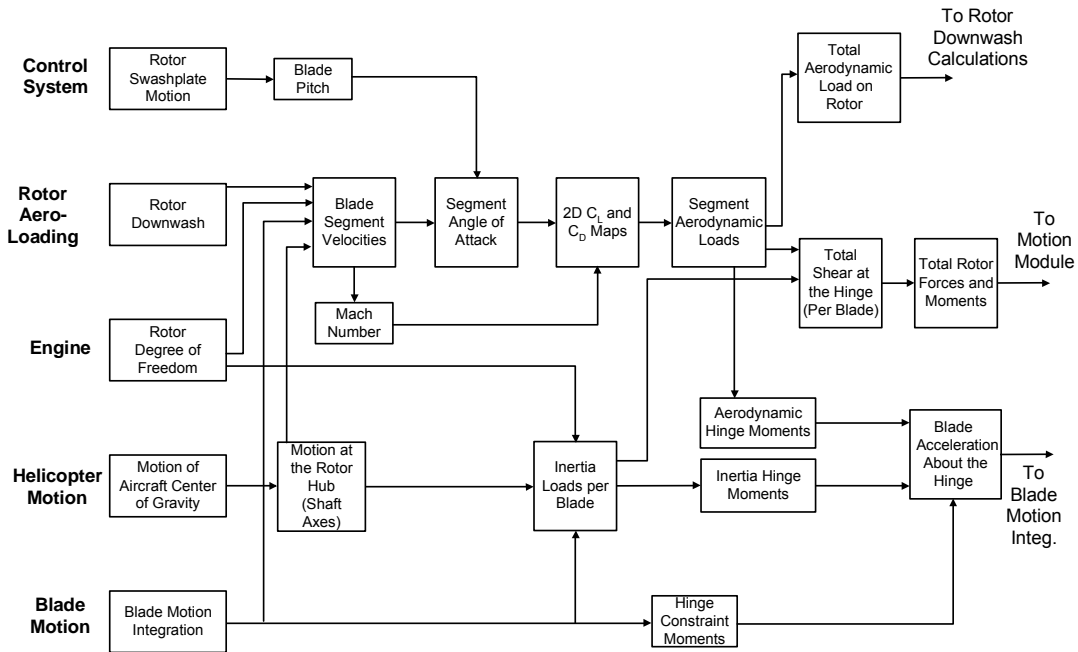


Figure 8 - Rotor blade element model flow diagram.

### 3.3.2. Coordinate Systems and Transformations

The following sections describe the coordinate systems used in the BER model and the transformations between them.

#### 3.3.2.1. Body and Hub Axes

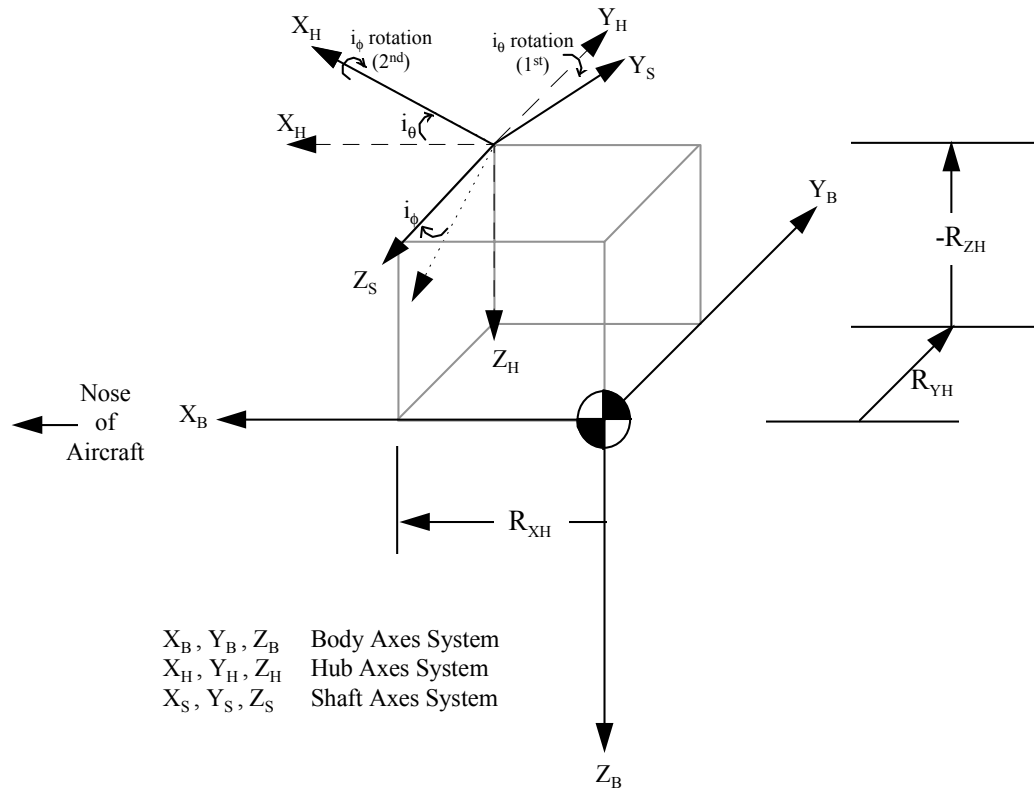


Figure 9 - Sketch showing body, hub and shaft axes coordinate systems.

Figure 9 shows the body axes, designated with the subscript  $B$ , along with the hub and shaft axes. The body axes emanate from the center of gravity, with the x body axis pointing forward, y body axis to the right and the z body axis down. This axis system is fixed to the aircraft. Typically, the states passed to the blade element model from the equations of motion are in body axes.

The hub axes, designated with the subscript  $H$ , are aligned with the body axes and translated through the radius  $\bar{R}_H$  emanating from the center of gravity and extending to the center of the rotor hub. Figure 9 shows the three components of vector extending from the center of gravity to the hub in the x, y and z body axes,  $R_{XH}$ ,  $R_{YH}$ , and  $R_{ZH}$ , respectively. Since both the translational velocity and acceleration are calculated by the equations of motion at the center of gravity, those quantities must be transferred to the hub axes.

### 3.3.2.2. Shaft Axes

Transformation from the body axes to the shaft axes, designated by the subscript  $s$ , is achieved using two Euler angles,  $i_\theta$  and  $i_\phi$ , respectively. These are the shaft tilt angles depicted in Figure 9 and represent a positive rotation of the shaft about the y hub axis followed by a positive rotation about the x shaft axis, respectively. Since these angles are Euler angles, the order of rotation described above must be maintained.

Once the rotor forces are calculated by the blade element routine, transformation from shaft axes back to hub axes is performed.

### 3.3.2.3. Rotating Shaft Axes

The rotating shaft axes, designated by the subscript  $RS$ , is a simple rotation of the shaft axes through the instantaneous azimuth angle of the blade. As shown in Figure 10 the rotating shaft axes are aligned with the fixed shaft axes when  $\psi=90^\circ$ . This coordinate system does not move with blade flapping or lag motion.

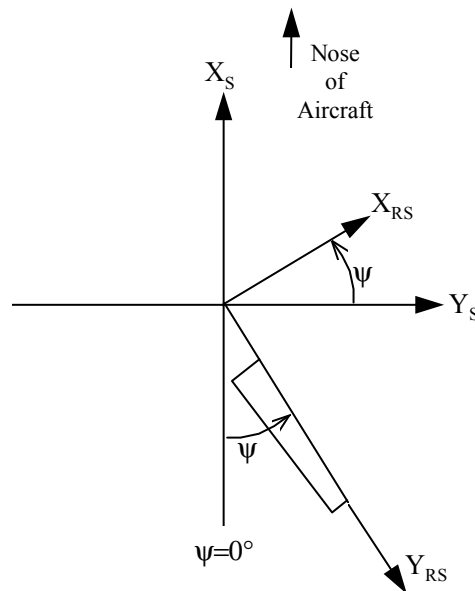


Figure 10 - Sketch showing the rotating shaft axes coordinate system.

### 3.3.2.4. Blade Element Axes

Transformation from the rotating shaft axes to the blade element axes, designated by the subscript  $BE$ , accounts for the two Euler angles that the blade rotates through. The first is the lag angle,  $\delta$ , followed by the flap angle,  $\beta$ . As Figure 11 shows,  $\delta$  is defined positive in the direction of blade rotation (in the 'lead' direction) and  $\beta$  is defined positive up.

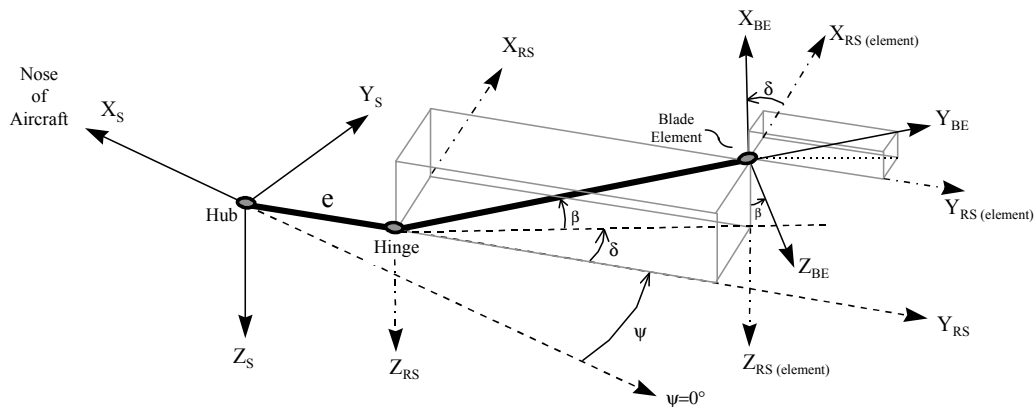


Figure 11 - Sketch showing the blade element axes coordinate system.

Although this is the final coordinate system transformation before actual calculation of the blade element forces is undertaken, a realignment of the direction of these forces is made to facilitate use of the two-dimensional airfoil data. This realignment defines the element forces in the tangential, perpendicular and radial directions.

### 3.3.3. Geometry of Blade Elements

#### 3.3.3.1. Rotation Angles

The rotation angles that the blade experiences, namely rotation angle,  $\psi$ , lag angle,  $\delta$ , and flap angle  $\beta$ , have been discussed in the previous section. However, no formal definition of these angles has been presented. Convention in the helicopter community defines  $\psi=0^\circ$  along the negative x shaft axis (blade pointed aft). In the current BER model,  $\psi$  increases with a counterclockwise rotation looking down on the rotor, as shown in Figure 10.  $\beta$  is defined positive up and  $\delta$  positive forward with respect to the rotating shaft axes. No explicit restrictions are placed on the harmonic content of the blade flap and lag angle during integration of the equations which govern those motions. However, it is often convenient to express  $\delta$  and  $\beta$  using a first order Fourier series expansion.

#### 3.3.3.2. Element Radial Location

The radial distribution of segments along the blade is determined by calculating the radial contours which define annuli of constant area. This concentrates elements toward the tip of the rotor where blade forces are highest. Before development of the expression for element radial location, it is convenient to nondimensionalize several quantities to simplify the equations and facilitate the use of these quantities in subsequent derivations. These nondimensionalized quantities are presented in Figure 12 and in the following relationships:

$$y = r / \underbrace{r_{\text{Tip}}}_{\text{RMR}} \quad \text{nondimensional rotor radial location}$$

$$\xi = \underbrace{e}_{\text{ZET}} / \underbrace{r_{\text{Tip}}}_{\text{RMR}} \quad \text{nondimensional hinge offset}$$

$$\xi' = (r_{\text{Cuff}} - e) / r_{\text{Tip}} \quad \text{nondimensional distance from hinge to blade root}$$

(nondimensional spar length)

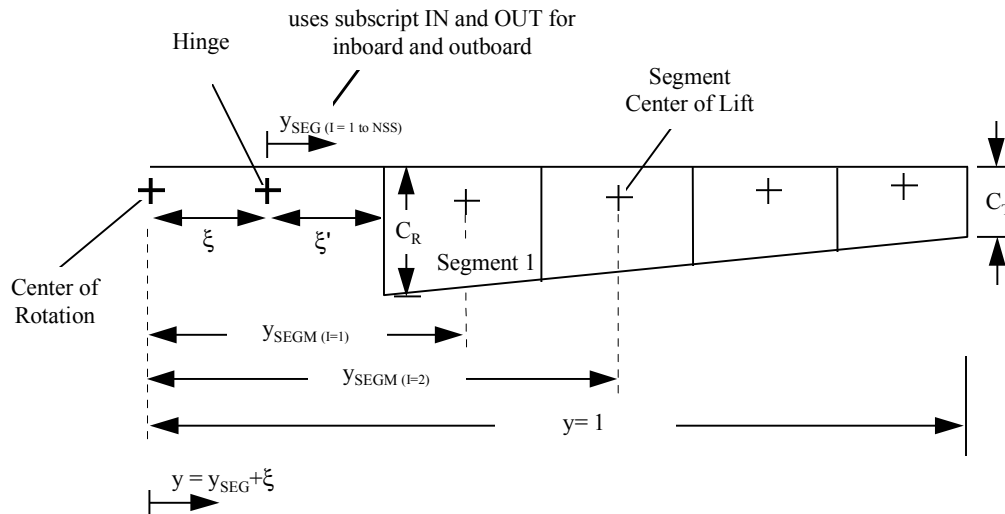


Figure 12 - Sketch showing blade segment geometry.

Using the relationships defined above and assuming linear blade taper, the geometry defining the blade element can be defined as follows:

### 3.3.4. Calculation of States Fixed with respect to Rotor

This section describes the quantities which do not vary with the radial or azimuthal location of a blade segment.

#### 3.3.4.1. Translational Velocity

The translational velocities experienced at the hub are equivalent to those at the center of gravity plus additional effects due to the body axis rotation vector.

#### 3.3.4.2. Translational Acceleration

Like translational velocity, the translation acceleration at the hub is equivalent to that at the center of gravity plus the addition effects that coupling between rotation and translational velocity at the center of gravity produces.

#### 3.3.4.3. Angular Velocity and Acceleration

Both the angular velocity and acceleration transfer directly from the center of gravity to the rotor hub. Therefore, these vectors need only transformation from hub axes to shaft axes coordinates.

### **3.3.5. Rotor Inflow Model**

The uniform downwash, calculated using momentum theory, is modified for ground effect and passed through a first-order lag. In addition, the uniform downwash is modified to account for a non-uniform distribution with forward airspeed. The non-uniform contributions to downwash are also passed through a first order lag. The following subsections present a brief discussion of the modeling for these effects.

#### **3.3.5.1. Modified for Ground Effect**

To account for ground effect, rotor thrust is multiplied by a factor which is a function of airspeed, rotor thrust and rotor height above the ground. This factor is equal to unity when the magnitude of the forward speed is greater than 40 knots.

#### **3.3.5.2. Application of Inflow Lag**

The downwash induced by the rotor lags behind the production of thrust when control inputs or flight conditions change on the actual aircraft. Therefore, a first order lag is placed on the uniform downwash calculation.

#### **3.3.5.3. Rotor-on-Rotor Interference**

The close proximity of the forward and aft rotors requires that an increment to downwash be included which accounts for the effect of the forward rotor on the aft rotor as well as the aft rotor effect on the forward rotor. This is done using tabular data which are used to calculate a downwash increment to one rotor based on the flight condition of the other.

### **3.3.6. Non Uniform Inflow**

The inflow distribution is not uniform on a maneuvering rotor or on a rotor in forward flight. A first harmonic approximation of the inflow distribution may be used to compensate for this.

The total expression for the non uniform downwash along the positive z shaft axis accounts for hinge offset, the lag degree of freedom and radial location of the blade element. The downwash velocity is resolved in blade element axes coordinates and used to calculate local angle of attack and velocity.

### **3.3.7. Element Model**

The majority of FORTRAN code that represents the mathematical modeling discussed up to this point is contained in the subroutine *BER*. This section begins discussion of the part of the blade element model which is specific to the individual blade and the integration of its elements along the blade and around the azimuth. The majority of the FORTRAN code for this portion of the discussion is contained in the subroutine *BLADE*. The following sections follow the flow of that subroutine wherever possible.

#### **3.3.7.1. Calculation of States Fixed Along Blade**

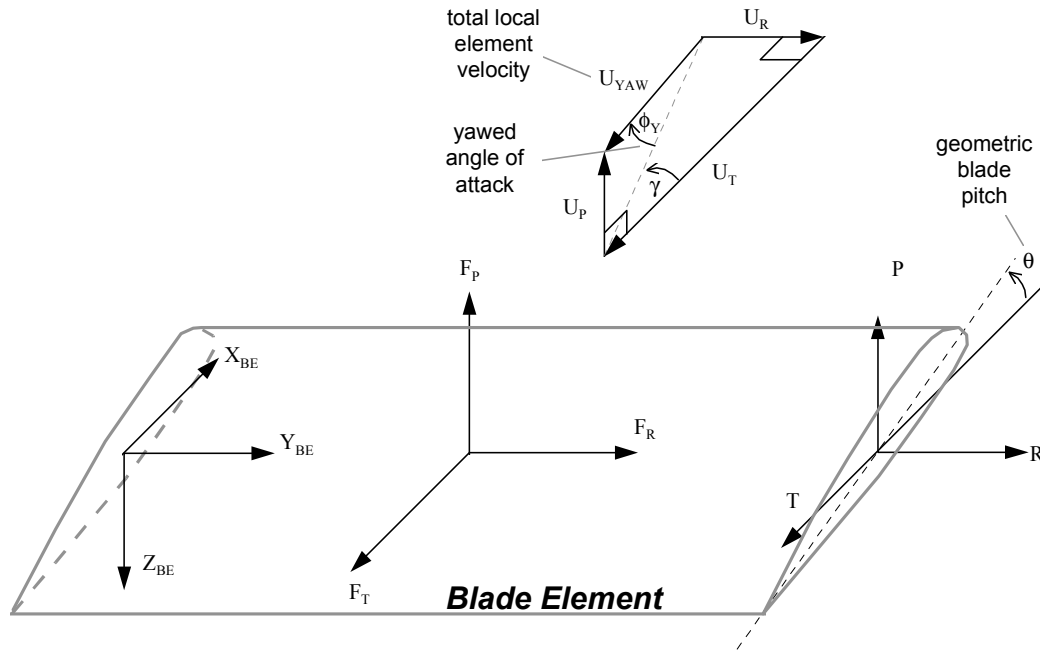


Figure 13 - Sketch showing local blade element velocity, angle of attack and forces.

Before a discussion of the equations governing the integration of rotor blade forces, it is necessary to define the direction of positive velocity components and forces acting on the blade element. As shown in Figure 13, the velocity components are defined in the tangential (negative  $X_{BE}$  axis), the radial (positive  $Y_{BE}$  axis) and the perpendicular (negative  $Z_{BE}$  axis). These three directions are designated by the subscripts  $T$ ,  $R$  and  $P$ , respectively. Defining the velocities in this manner facilitates the formulation of the local angle of attack and use of the two-dimensional lift and drag data, as described in the remainder of this section. The local lift and drag forces (initially described in local element wind axes coordinates) are resolved in the components corresponding to the tangential, radial and perpendicular directions and converted to hinge shear forces and moments.

### 3.3.7.2. Calculation of Velocity Components Fixed Along Blade

The nondimensional translational velocity equations must first be transformed to account for blade flap and lag angles. In addition, the constant velocity along the blade must also account for the translational velocity of the flap hinge due to the combination of angular velocity of the aircraft and the hinge offset.

### 3.3.7.3. Calculation of Local Element States

With the local velocity components that are constant along the blade defined, the quantities which vary along the span of the blade can be defined and combined with those described in previous sections to determine the lift and drag acting on each two-dimensional blade segment.

### **3.3.7.3.1. Geometric Pitch**

The geometric pitch of the blade is a function of several factors, not necessarily a function of radial position. The first is the geometric twist of the blade,  $\theta_T$ . In most helicopters, the twist is linear meaning that the variation of blade twist along the span is constant. In addition to linear twist, the blade element model allows for a table lookup as a function of blade span for those helicopters that employ nonlinear blade twist. The current blade element model also allows for dynamic blade twist (twist in addition to geometric twist caused by blade loading), however, this option is currently disabled and will not be discussed.

The second factor determining blade pitch is pilot input. The third and final contribution to blade pitch is the kinematic pitch coupling due to flapping, or  $\delta_3$  effect. This effect is a positive rotation of the blade pitch axis,  $\delta_3$ , about the vertical rotating shaft axis. Therefore, in the BER model positive  $\delta_3$  causes a decrease in blade pitch proportional to a positive increase in flap angle. Pitch-lag coupling is not included in the current BER model. The total blade pitch angle is then determined for each individual segment along with blade twist.

### **3.3.7.3.2. Local Segment Velocities**

The components of velocity which do not change along the span of the blade have been previously described in Section 3.3.7.2. However, before expressions for the total segment velocity components  $U_T$ ,  $U_R$  and  $U_P$ , shown in Figure 13, can be presented, the velocity components induced by both body and blade rotation rates must be developed. These rates can be transferred directly to the blade hinge, but must be transformed through the total angular displacement of the blade about the vertical shaft axis, or  $\psi + \delta$ . Figure 14 shows this transformation. Two angular velocity terms in addition to those of the body are added to account for blade rotation rate about the shaft,  $\Omega$ , and the blade lagging rate,  $\dot{\delta}$ .



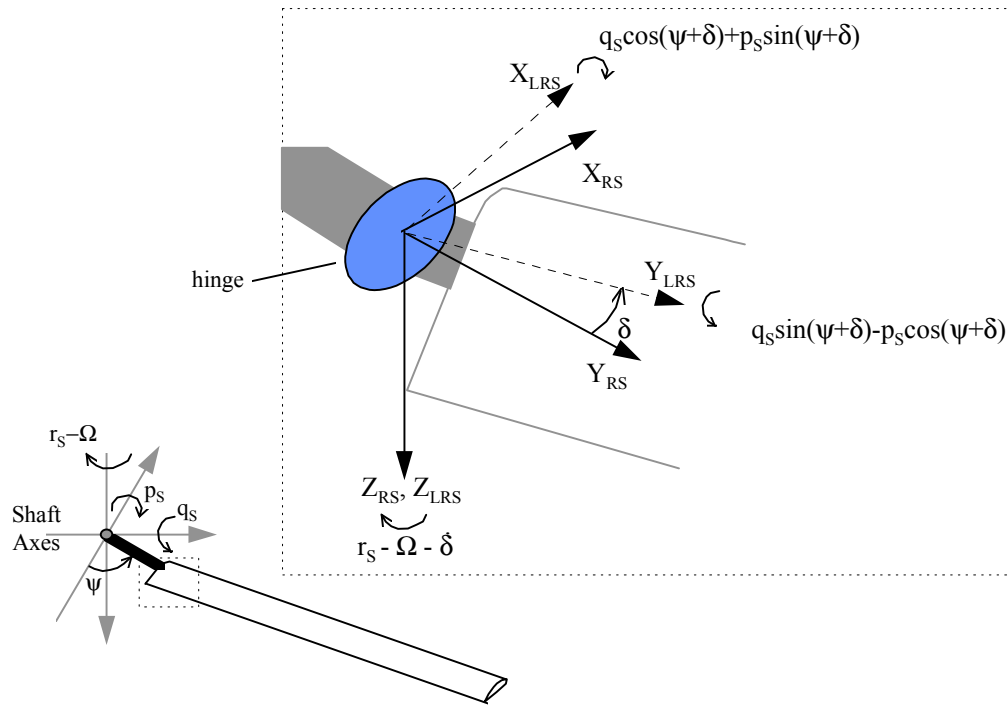


Figure 14 - Sketch showing angular velocity transformation from hub to hinge.

The velocity induced at the blade element by the hinge angular rates can be calculated by taking the vector product of the hinge angular rate,  $\omega_{LRS}$  and the radius extending from the hinge to the element,  $r_{BE}$ .

The total tangential, radial and perpendicular velocity components are then determined. In addition, the tangential, radial and perpendicular components of the turbulence velocity (gust) are included.

According to compressible flow theory for swept wings, when calculating the Mach number, the radial flow component is not considered. Therefore, the local Mach number for the segment, used in airfoil data table lookups, is given by the following relationship:

$$\underline{M}_{AMACH} = \sqrt{\underbrace{U_T^2 + U_P^2}_{UN}} \underbrace{\frac{V_{Tip}}{a}}_{XKR34} \quad (3.32)$$

### 3.3.7.3.3. Segment Angle of Attack and Application of Sweep Theory

The velocity components described above are pictured in Figure 13. In order to calculate the segment angle of attack from the velocity components described above, it is necessary to resolve the yawed tangential and perpendicular velocity components ( $U_N$  and  $U_P$ ) into components normal and parallel to the segment

chord. In addition, the segment blade pitch must be rotated through the angle  $\gamma$  so that it is in the plane of  $U_N$  and  $U_P$ . Figure 15 shows the streamwise blade pitch angle,  $\theta_Y$ , along with the tangential and radial velocity components.

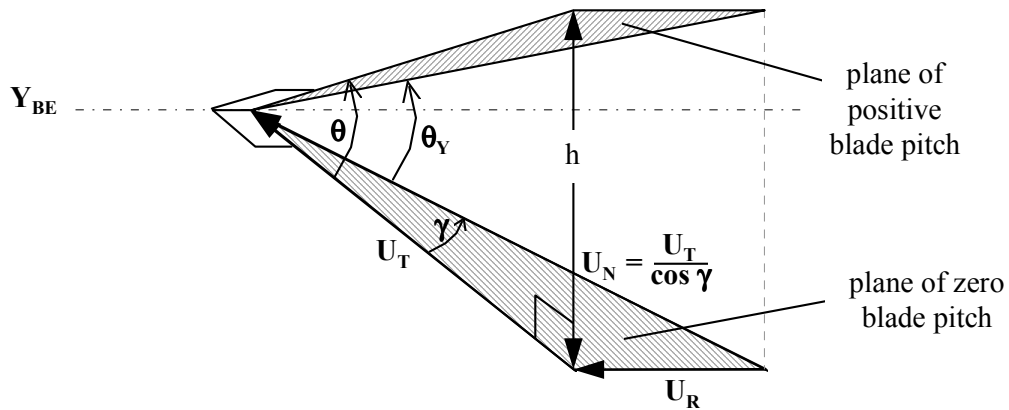


Figure 15 - Sketch showing orientation of segment streamwise blade pitch angle.

From Figure 22 it can be seen that the following two expressions for the tangent of the respective blade pitch angles can be expressed as follows:

$$\tan \theta = \frac{h}{U_T} \quad \text{and} \quad \tan \theta_Y = \frac{h}{U_T / \cos \gamma} = \frac{h \cos \gamma}{U_T}$$

therefore,

$$\tan \theta_Y = \underbrace{\tan \theta}_{\text{THSUM}} \overbrace{\cos \gamma}^{\text{CGAM}} \tag{3.33}$$

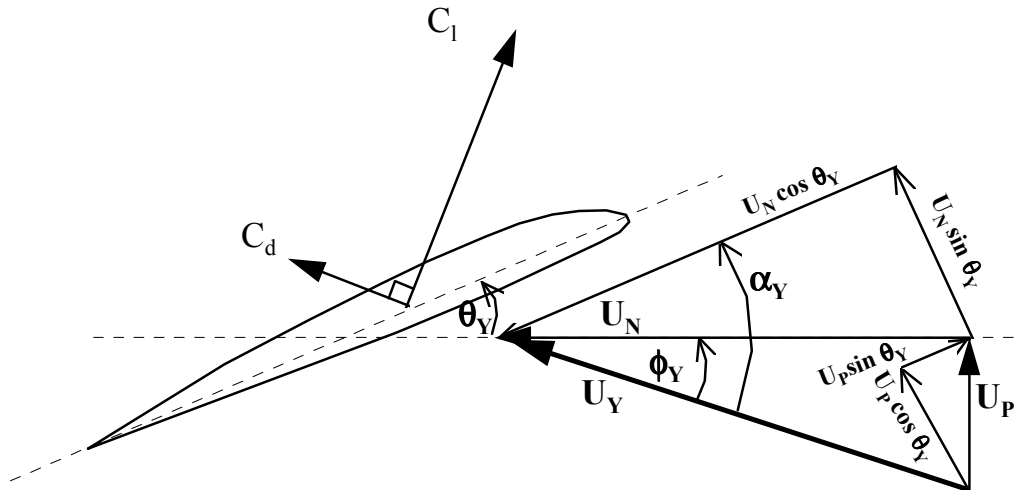


Figure 16 - Resolution of local velocity components into the streamwise blade pitch axes.

Figure 16 shows the yawed tangential and perpendicular components of the flow resolved into components aligned with the streamwise blade pitch angle. The total angle of attack of the segment,  $\alpha_Y$ , is then determined.

### 3.3.7.4. Calculation of Element Local Lift and Drag Coefficients

The following sections describe the two methods currently implemented in the blade element rotor model to calculate local lift and drag coefficients,  $C_l$  and  $C_d$ . These are controlled using the FORTRAN variable AERCHAR, where AERCHAR is set to 0 for the simplified model and set to 2 to use the nonlinear airfoil tables. The option which uses C-81 style tables (AERCHAR = 1) is not currently implemented.

#### 3.3.7.4.1. Simplified Model (AERCHAR = 0)

The simplified model multiplies the square of the angle of attack by a coefficient,  $\delta_1$  plus a minimum drag coefficient,  $\delta_0$  to get element drag coefficient,  $C_d$ . No attempt is made to apply sweep theory to correct  $C_d$  in the simplified model.

Lift coefficient is calculated by multiplying a constant lift curve slope by a corrected angle of attack,  $\alpha_{TRANS}$ . The linear region is defined by the negative and positive angle of attack limits,  $\alpha_{CL3}$  and  $\alpha_{CL1}$  respectively. The transformed angle of attack,  $\alpha_{TRANS}$ , is calculated using simple sweep theory. Because sweep theory does not apply at high angles of attack,  $\alpha_{TRANS}$  is held constant above and below  $\alpha_{CL1}$  and  $\alpha_{CL3}$ .

#### 3.3.7.4.2. Table Lookup to Determine $C_l$ and $C_d$ (AERCHAR = 2)

The method to calculate  $C_l$  and  $C_d$  described above is useful for limited cases where the rotor is operating in the linear region, or when a decrease in

computational time is required. However, it does not allow for accurate prediction of the aerodynamic forces for high-speed/high-thrust conditions where compressibility, reversed flow, stall and other nonlinear effects can dominate various regions of the rotor as it rotates. In these cases, rotor airfoil data are contained in separate files for  $C_l$  and  $C_d$  as functions of both local angle of attack and Mach number. No transformation of  $\alpha_Y$  is made before interpolation of the data tables is executed.

### **3.3.8. Calculation and Summation of Blade Angles, Forces and Moments**

With the lift and drag coefficients defined for the blade, along with the element geometry and local velocity components, it is possible to integrate the forces acting along the blade. The resulting aerodynamic forces and moments are resolved into several components which represent the shear loads at the hub and the moments about the flap and lag hinges. The following discussion presents the relationships which are used to calculate the forces and moments at the hub due to blade aerodynamics, inertia and hinge constraints.

#### **3.3.8.1. Normal, Tangential and Radial Aerodynamic Forces of a Blade Element**

Figure 16 shows the direction of the lift and drag vectors acting on the blade element. The direction of these vectors is dependent only on the local induced angle of attack,  $\phi_Y$ , not the blade pitch angle,  $\theta_Y$ . Inspection of Figure 16 indicates that resolution of  $C_l$  and  $C_d$  into the perpendicular and tangential directions is relatively simple.

#### **3.3.8.2. Total Aerodynamic Hinge Moments and Blade Shears in Rotating Shaft Coordinate System**

##### **3.3.8.2.1. Aerodynamic Flapping and Lagging Moments About Hinge**

The aerodynamic flapping and lagging moments about the hinge are products of the radial distance from the hinge to the blade element midpoint and the perpendicular and tangential blade forces, respectively. Since the radial blade force is aligned with the blade span axis, it has no effect on the flapping or lagging moment.

##### **3.3.8.2.2. Aerodynamic Shears**

In order to calculate the aerodynamic shears at the hinge in rotating shaft axes coordinates, it is necessary to transform the tangential, radial and perpendicular blade forces from the blade axes to rotating shaft axes coordinates.

##### **3.3.8.3. Flap and Lag Angle Calculation**

Hinge constraint moments generated by spring and damping effects at the flapping and lagging hinge are used to determine flapping and lagging accelerations. For both flap and lag, simple first order differential equations describe the respective moments. Fundamentally, these equations state that the sum of the moments acting on a body is equal to the time rate of change of its angular momentum.

### **3.3.8.3.1. Flap Angle**

The equation used in the BER model to solve for rotor flapping acceleration,  $\ddot{\beta}$ , neglects terms containing body rate products and small blade angular products. The original blade element model included in GenHel used an integration scheme which assumed first harmonic flapping behavior and, therefore, could tolerate large integration time steps. This was done to ensure real-time performance on the current technology computers of the time. However, for certain conditions this integration scheme proved unsuitable. Utilizing the increased computational capabilities of current technology computers, a second order Adams-Bashforth integration technique (AB-2) was employed to increase model fidelity without compromising real-time run capability. The AB-2 integration scheme uses the derivative of the current time step along with the derivative from the previous time step to calculate the effective rate of change over the time step to integrate  $\ddot{\beta}$  and  $\dot{\beta}$  to solve for flap angle.

### **3.3.8.3.2. Lag Angle**

The comprehensive relationship describing lagging acceleration,  $\ddot{\delta}$ , is similar to that of the flapping acceleration. Also like flapping, the lagging acceleration equation incorporated in the blade element model neglects terms such as body rate products and small blade angular products. Also like flapping, the original integration scheme used in the GenHel model was replaced with an Adams-Bashforth integration routine. However, a third order integration technique, AB-3, was needed to ensure stability of the blade lagging motion without compromising real-time run capability. The AB-3 integration scheme uses the current derivative along with the derivative from the two prior time steps to integrate  $\ddot{\delta}$  and  $\dot{\delta}$  to solve for lag angle. The lag degree of freedom can be turned off thus yielding  $\delta = \dot{\delta} = \ddot{\delta} = 0$ .

### **3.3.8.4. Inertial Shears, Total Shaft Shears and Total Hub Moments**

#### **3.3.8.4.1. Calculation of Inertial Shears**

The governing equation which defines the inertial shear Force,  $F_H$ , at the hinge due to blade motion is presented in the following equation:

$$m_b \bar{a}_{cg} = -\bar{F}_H \quad (3.34)$$

where  $\bar{a}_{cg}$  is the acceleration of the blade center of gravity in rotating shaft axes coordinates. This equation requires the acceleration of the blade at its center of gravity. Again, cancellations of body rate and small blade angular product terms from the resulting equations yields the blade inertial shears at the hinge in rotating shaft axes coordinates.

#### **3.3.8.4.2. Calculation of Total Shaft Shears**

The total hinge shear force components for each blade are described by summing the aerodynamic shear force components and the inertial shear force components. The total shaft shear force must be calculated by summing the individual contribution from each blade. This requires that each component be transformed to fixed shaft axes coordinates before it is summed. These shaft forces are thrust,  $T_H$  (positive up), horizontal force,  $H_H$  (positive aft) and lateral force,  $J_H$  (positive to the left). To maintain consistency with other simulation subroutines, the total hub shears must then be transformed to aircraft wind axes coordinates. It should be noted that the sideforce in wind axes coordinates,  $Y_R$ , is positive to the right making it the opposite sign of  $J_H$ .

#### **3.3.8.4.3. Calculation of Total Hub Moments**

Similar to the summation of the total shear forces, the total hub moments must be summed for each blade in fixed shaft axes coordinates. This is further complicated by the hinge spring and damper moments which are not expressed in rotating shaft axes coordinates. Therefore, these moments must first be transformed to rotating shaft and then to fixed shaft axes coordinates before being summed into hub moments. The moments created by the vector product of the rotor hinge shear and the hinge offset,  $e$ , results in expressions for the total x, y and z hub moments in fixed shaft axes coordinates. As was the case with the hub shears, the total hub moments must be transformed to aircraft wind axes coordinates to maintain consistency with other simulation subroutines.

### **3.4. Fuselage Aero Forces And Moments And Total Force And Moment Summation**

#### **3.4.1. Determination Of Fuselage Aero Forces And Moments**

As indicated earlier, fuselage forces and moments (Figure 17) are determined from tabular body axis coefficient data, which is based upon rotor OFF "drag model" wind tunnel results. Input arguments for fuselage table look up are fuselage angle of attack and sideslip,  $\alpha_{FUS}$  and  $\beta_{FUS}$ , respectively. The  $\alpha_{FUS}$  term includes an average rotor downwash term that is applied to the total linear velocity component.

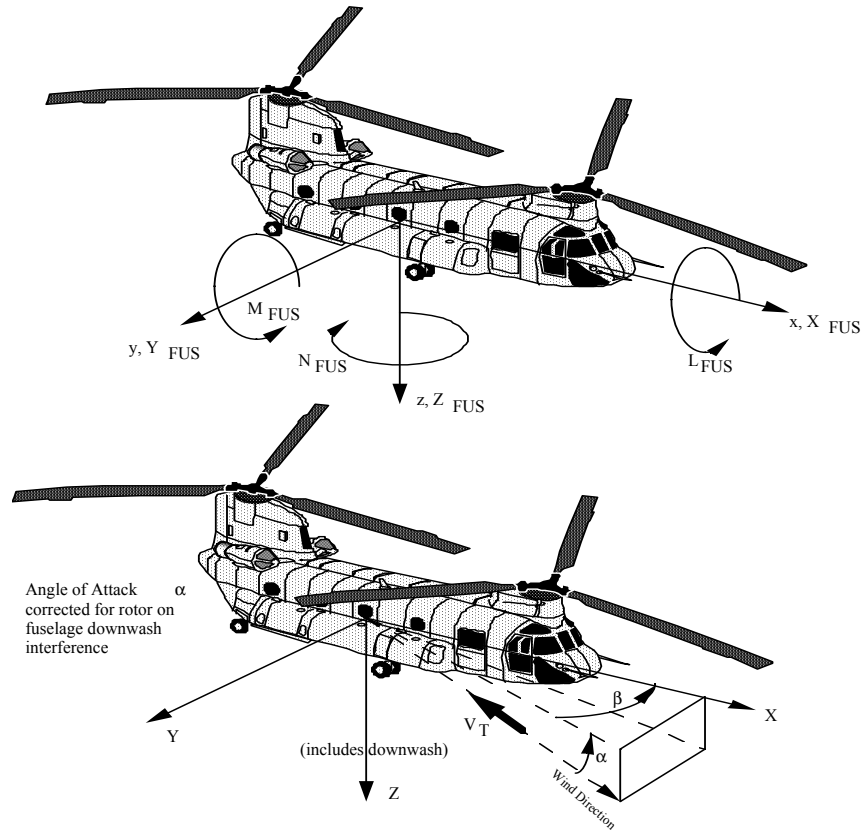


Figure 17 - Fuselage Forces and Moments

With the downwash-corrected  $\alpha_{FUS}$  and  $\beta_{FUS}$  arguments and local dynamic pressure,  $q_{FUS}$  computed, the lift, drag, side force, and pitching, rolling and yawing moment data are extracted from the tables. Sign convention for these parameters is shown in Figure 17. These results are then corrected to the desired aircraft equivalent flat plate area ( $f_e$ ). Further corrections account for differences between the aircraft C.G. location selected for simulation, and the position of the force and moment center about which the tabular wind tunnel results were derived.

Forces and moments are calculated in the final program step by multiplying the corrected coefficients by  $q_{FUS}$ . The sequential steps followed in computing these fuselage aero parameters are discussed next. (Note that  $q_{FUS} = 1/2 \rho V_{TOTfus}^2$ ).

#### 3.4.1.1. Determination of Fuselage Angle of Attack, Sideslip, and Local Dynamic Pressure

Average lagged rotor downwash  $\bar{v}$  (called WIFS in the program) is added to the total airframe vertical velocity component ( $W_T$ ) to correct the fuselage flow for rotor effects. Local fuselage quantities,  $q_{FUS}$ ,  $\alpha_{FUS}$  and  $\beta_{FUS}$  are then computed using the following expressions:

$$w'_T = W_T + W_{IFS} \quad (3.35)$$

$$(w'_T)^2 = (W_T)(W'_T) \quad (3.36)$$

$$u_T^2 = (u_T)(u_T) \quad (3.37)$$

$$v_T^2 = (v_T)(v_T) \quad (3.38)$$

$$V_{TOT_{FUS}} = \sqrt{(W'_T)^2 + u_T^2 + v_T^2} \quad (3.39)$$

$$q_{FUS} = \frac{\rho}{2} (V_{TOT_{FUS}})^2 \quad (3.40)$$

$$\alpha_{FUS} = \tan^{-1} \frac{w'_T}{u_T} \quad (3.41)$$

$$\beta_{FUS} = \tan^{-1} \frac{v_T}{u_T} \quad (3.42)$$

sine and cosine of  $\beta_{FUS}$  are then compiled for later application in interpolating between the  $\beta = 0^\circ$  and  $\beta = 90^\circ$  DF curves, which are used in the computation of rotor inflow ratio  $\lambda$ .

#### **3.4.1.2. Table Lookup for Fuselage Force and Moment Coefficients**

Nondimensional fuselage aero data are stored as coefficients in the form:  $L/q$ ,  $D/q$ ,  $Y/q$ ,  $M/q$ ,  $L/q$ , and  $N/q$ ; which represent respectively, lift, drag, side force, pitch, roll, and yaw moment. Coefficients are dimensionalized by multiplying these terms by the local dynamic pressure by  $q_{FUS}$ . Sign convention for these parameters is as follows:

D	=	Drag Force	(Positive Aft)
L	=	Lift Force	(Positive Up)
Y	=	Side Force	(Positive Right)
M	=	Pitching Moment	(Positive Nose Up)
L	=	Rolling Moment	(Positive Roll Right)
N	=	Yawing Moment	(Positive Yaw Right)



### **3.4.1.3. Equivalent Flat Plate Area ( $\Delta f_e$ ) Corrections**

Wind tunnel fuselage aero data frequently does not account for such things as rotor hub drag, momentum drag losses, leakage drag, and the drag associated with installation of engine inlet protection screens. An equivalent flat plate area ( $\Delta f_e$ ) correction is applied to the tabulated lift, drag, and side force coefficient data to account for these items. In the case of the CH-47B wind tunnel, the  $\alpha = \beta = 0^\circ$  drag ( $f_e$ ) is 24.88 ft.<sup>2</sup> (see Table A-1), whereas the total flat plate drag of the RAF HC MK2 (without engine inlet screens) is 50.0 ft.<sup>2</sup> It should be noted that the RAF HC MK2 aircraft is configured with all weather screens, therefore a  $\Delta f_e$  of 7.0 ft.<sup>2</sup> is added to account for their parasite drag increment.

Based upon the 50.0 and 24.88 ft.<sup>2</sup> drag values, a  $\Delta f_e = 25.12$  ft.<sup>2</sup> correction must be applied to the wind tunnel tabular results for the RAF HC MK2 helicopter. This  $\Delta f_e$  correction is expressed in the wind axis, and hence must be referred to the fuselage body axis through a transformation which accounts for  $\alpha_{FUS}$ , and  $\beta_{FUS}$ .

### **3.4.1.4. Wind Tunnel Moment Arm Correction and Calculation of Fuselage Forces and Moments From Coefficients**

Final fuselage force data (expressed in pounds) are calculated by multiplying the local  $q_{FUS}$  by the tabular  $D/q$ ,  $Y/q$ ,  $L/q$  forces corrected for the  $\Delta f_e$  terms  $\Delta X/q_{FPC}$ ,  $\Delta Y/q_{FPC}$  and  $\Delta Z/q_{FPC}$ .

Sign changes in the equations account for the axis conversion from fuselage  $D$ ,  $Y$ , and  $L$  (which are positive in a rearward, right, and upward direction) to  $X$ ,  $Y$ , and  $Z$  which are positive forward, right, and down for the airframe E.O.M.

Tabular moment data listed in the wind tunnel tables are expressed about some scaled C.G. position (usually the model mounting trunnion center), which generally does not agree with the aircraft C.G. selected for simulation purposes. Accordingly, a longitudinal ( $1c$ ), vertical ( $hc$ ), and lateral ( $dc$ ) moment arm correction (i.e. the distance between the wind tunnel C.G. and the simulation aircraft C.G. in feet) must be applied. This is done by multiplying these arms by the appropriate fuselage force components, to account for the moment of these forces in the overall fuselage moment totals. The complete dimensionalization with  $q_{FUS}$  and correction for wind tunnel C.G. offset is then performed.

In the multiplication of moment arms by the body axis forces, positive directions for  $l_c$ ,  $h_c$ , and  $d_c$  (called SLCFS, SHCFS, and SDCFS in the program) locate the model center forward, above, and to the right of the aircraft center of gravity.

### **3.4.1.5. Accountability For Rearward Flight**

When the aircraft is in forward flight, the forces and moments computed above utilize the same signs as calculated. In rearward flight, three sign corrections to those initially computed are required. These change the sign of  $X_{FUSE}$ ,  $M_{FUSE}$ , and  $N_{FUSE}$ .

### **3.4.2. Resolution Of Rotor Forces And Moments Into The Aircraft Body Axis And Summation With Fuselage Data**

#### **3.4.2.1. Moment of Rotor Forces With Resolution of Forces and Moments Into Body Axis**

All individual fuselage and rotor forces and moments have now been computed, except for the moments imposed upon the airframe (about its C.G.) by the rotor T, H, and Y forces. Rotor forces and moments are computed in the S.N.P. wind axis, whereas the fuselage data is referred to the aircraft body axis when calculated. In order to determine the moment contributions of the rotor forces, it is first necessary to resolve T, H, and Y through the rotor ( $\beta'$ ) sideslip and (i) shaft incidence angles back into the airframe body axis (it is important to note that if the blade element rotor model was used to generate these rotor forces,  $\beta'$  is zero for both rotors). With this resolution completed, rotor moment arms (h, l, and d) are multiplied by the forces to produce the moment of these forces in the body axis.

Rotor hub flapping moments (and torque) are next resolved into the body axis through  $\beta'$  and i; and these moments are then summed with those produced by the forces at the hub to derive the final total.

The final manipulation of rotor hub moments resolves L, M, and Q back through rotor sideslips,  $\beta'$ , and shaft incidence, i into the airframe body axis. These hub moments are later summed with rotor force and fuselage moments preparatory to executing the equations of motion. Note in this transformation that the torque applied to the airframe is the torque supplied by the forward rotor shaft dynamic system ( $Q_{GOV}$ ), and not the classical equation aero torque required ( $Q_{AERO}$ ), as might be suspected. This shaft dynamic system torque is provided by a second order rotor dynamics model.

#### **3.4.2.2. Summation of Rotor and Fuselage Forces and Moments**

The rotor forces and moments resolved into the body axis are now added to the fuselage force and moment totals previously calculated. The final sum of all these aero forces and moments is then available for application in the rigid body equations of motion (described earlier at the beginning of this section of the report). Combining the rotor and fuselage force and moment totals is then accomplished

## **4. AIRCRAFT DYNAMIC SUBSYSTEMS**

### **4.1. Mechanical Controls Model**

A brief introduction to the RAF HC MK2 flight controls design is presented and includes a description of how the tandem helicopter control system is used to maneuver the aircraft (Figures 18 and 19). Note, the tandem helicopter control mechanization varies significantly from that employed in conventional single rotor helicopters.

#### **4.1.1. Tandem Rotor Helicopter Flight Controls Scheme**

The tandem rotor helicopter utilizes cockpit stick and pedal control inputs to maneuver the aircraft in a somewhat different manner than is characteristic of the single rotor configuration. Collective and lateral cyclic control functions are similar for both types of aircraft, but the longitudinal/pitch and directional axis control schemes are substantially different. Except for longitudinal trim functions discussed later, the tandem helicopter rotor system uses only two types of pitch control at the rotor head - collective and lateral cyclic.

These control inputs are produced by two hydro-mechanical actuators located 180 deg apart beneath the swashplate. Both actuators move together to produce ( $\theta_0$ ) collective pitch control, and differentially to tilt the swashplate for lateral cyclic input.

The final rotor control is utilized as a trim function to reduce fuselage nose down attitude at high speed and undesirable longitudinal aerodynamic flapping which can create excessive hub pitching moments. On the RAF HC MK2, this control function is produced with a very slow "q" (dynamic pressure) sensed electro-mechanical actuator. Longitudinal cyclic control is not available to the RAF HC MK2 pilot through the cyclic stick (as it is with single rotor aircraft), but is added at the swashplate through a separate actuator, which is not grounded to the airframe in the same manner as the upper boost actuators are. The longitudinal cyclic pitch trim is an AFCS function.

Aircraft directional, lateral, vertical, and longitudinal responses to the tandem rotor controls described above are covered in the following sections, respectively.

#### **4.1.2. Directional Control**

Anti-torque compensation is not a problem with the tandem helicopter since the torque produced by its counter-rotating rotors tends to cancel out. Thus both rotors are fully available for the directional control task since neither has a full time anti-torque requirement (like the tail rotor on a single rotor machine). Moreover, there is not a power penalty to achieve anti-torque trim for the tandem configuration. In the tandem rotor vehicle, directional control is achieved through application of differential lateral cyclic pitch on each rotor. Pedal inputs tilt the

forward and aft rotor thrust vectors in opposite directions laterally, and thus produce a directional moment (couple) to turn the aircraft. Because the tandem aircraft has a relatively large directional inertia and the control of this axis is limited to differential lateral cyclic, it has the lowest bandwidth with respect to the other control axes. However, the dynamic response for the CH-47 has proven to be operationally sufficient.

Tandem helicopter rotor response to directional control is illustrated in Figure 18. Also shown in Figure 18 is the response of the rotor system to a lateral stick input, which is discussed below.

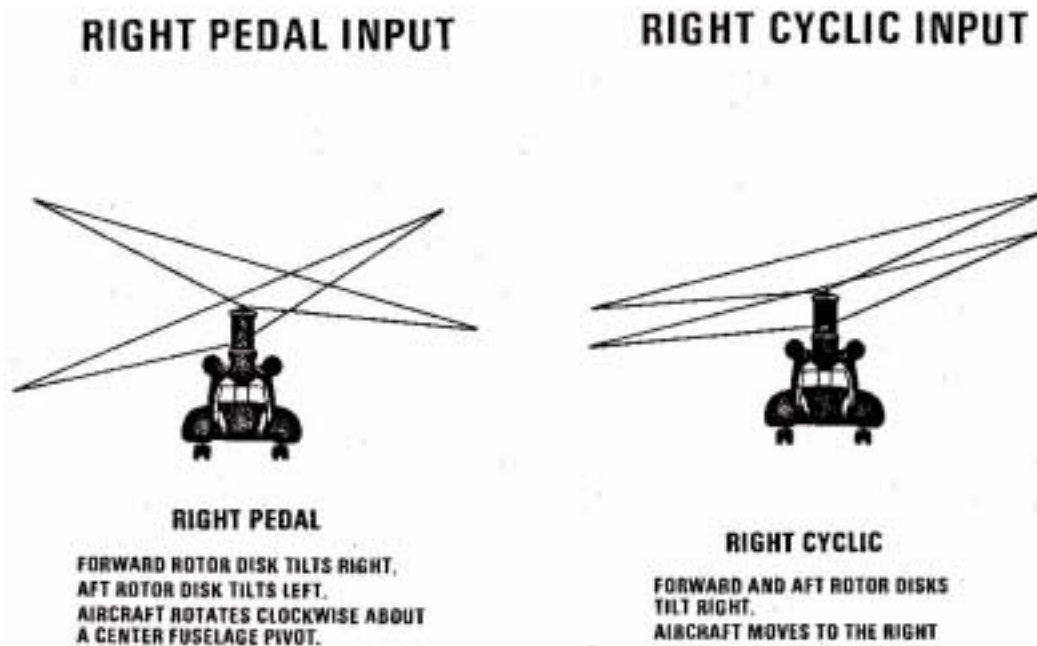


Figure 18 - Tandem Rotor Response to Directional and Lateral Control

#### 4.1.3. Roll Control

Roll control of the RAF HC MK2 aircraft is achieved through the introduction of identical lateral cyclic pitch commands to both forward and aft swashplates. Right cyclic stick input produces rotor thrust tilt to the right, as shown in Figure 18. This thrust tilt is achieved with a positive cyclic input to the forward rotor, and a negative command to the aft. Opposite signs are required because of the opposite rotational sense of each rotor. Since positive cyclic produces downward flapping on the advancing side of both rotors (and the advancing sides are opposite one another), negative cyclic is required at the rear rotor to produce lateral flapping to the right in response to a right stick input.

#### **4.1.4. Vertical Control**

Vertical control is the least complex of those employed on the tandem aircraft. Movement of the collective lever increases the collective pitch of all rotor blades on both rotors by the same amount, as illustrated in the sketch on the upper right side of Figure 19. Increasing collective pitch on both rotors produces an identical positive thrust delta on each, with an attendant increase in coning (and vertical speed when the aircraft is in the hover or low speed mode).

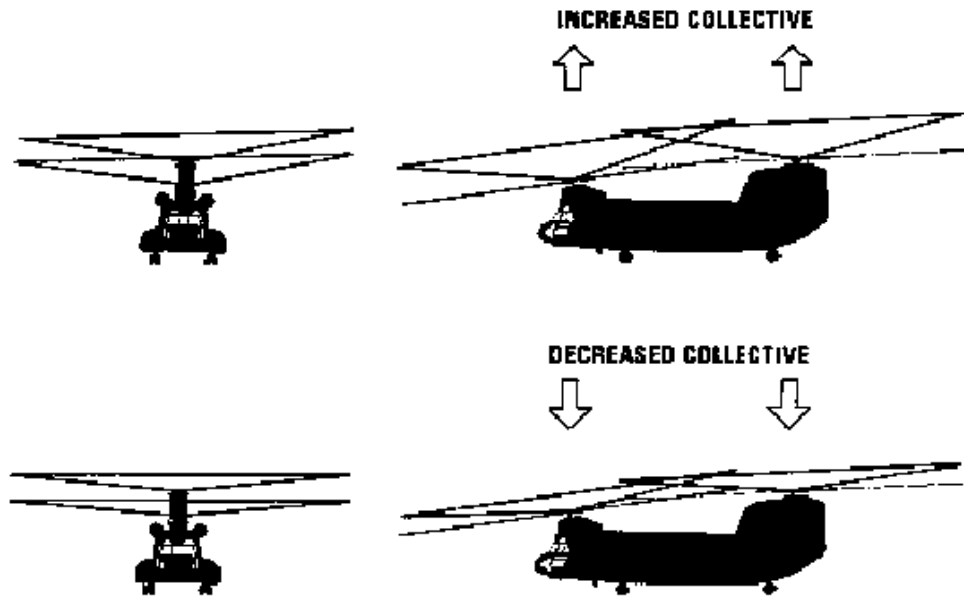
In forward flight, collective pitch changes are made in order to trim the aircraft at various speeds in accordance with the power required trend. Positive collective control is also used for steady state turns in level flight to produce more thrust, so that the vertical component of lift will equal the weight of the vehicle.

#### **4.1.5. Longitudinal Pitch Control**

To control the RAF HC MK2 tandem helicopter in pitch, differential collective pitch (DCP) is applied to both rotor heads. Longitudinal cockpit stick inputs increase collective pitch on one rotor and decrease it by the same amount on the other. For a forward stick input, DCP will cause a decrease in forward rotor thrust, and a corresponding increase on the rear rotor. Since differential thrust is essentially an acceleration control, once the desired nose down pitch attitude is reached, the longitudinal stick must be neutralized to hold this pitch angle. The longitudinal stick trim trend is a steady migration forward with increasing airspeed. This positive static stability is achieved through the displacement of the AFCS DASH actuator in series with the longitudinal axis mechanical control path.

If there were only DCP to control the longitudinal axis, then the faster the aircraft traveled, the more nose down the fuselage would become. This occurs because the increased  $q$  at higher speed produces more fuselage drag, which can only be overcome with greater (forward) tilt of the thrust vectors to produce more propulsive ( $X$ ) force. Since the thrust vector direction governed by the controls available to the pilot is virtually fixed with respect to the fuselage, the only way to achieve more propulsive force is to pitch the aircraft over further. Therefore, as introduced earlier, automatic,  $q$ -sensed longitudinal cyclic pitch trim is used to mitigate this nose down tendency with increasing speed. The use of additional airspeed-scheduled forward cyclic permits a moderation in the nose down attitude required to overcome airframe drag.

### Collective Inputs



### Forward Pitch Stick Input

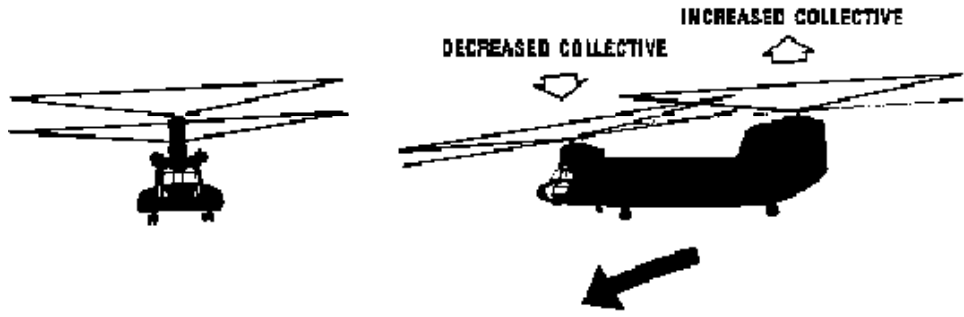


Figure 19 - Tandem Rotor Response to Collective and Longitudinal Control

#### **4.2. Automatic Flight Control System (AFCS) Model**

The AFCS model for the RAF HC MK2 is available with this simulation model. The AFCS and all mechanical control laws are modeled using the Boeing proprietary digital modeling tool VisVec (Visual VECEX).

VECEX is a real-time simulation modeling language tailored for emulation of dynamic systems elements through a macro-based format. It has the advantage of facilitating rapid prototyping of control system designs since the user need only chain macros together and supply an execution vector for an overall list of all specific macros (nodes) used. In addition, VECEX has the benefit for the

design that it is an interpretive language so that recompilation is not required following revision to the code. It allows the designer to revise existing nodes, add new nodes, or delete existing nodes without recompilation. It has been configured for real time operation at Boeing. In addition, since the VisVec graphical tool has been configured to produce VECEX code, the simulation model can be graphically specified. The contents of the library of algorithms available to the designer are referred to as macros (e.g. an integrator), while specific applications of a macro (e.g. an integrator with a specific gain and input definition for the longitudinal AFCS) are referred to as nodes. For the purposes of the simulation model delivered for the Netherlands, these macros were recoded in C to provide a standalone capability not requiring the VisVec tool.

Note that the AFCS control laws are executed in analog hardware on the aircraft. Many limits are in fact amplifier saturation levels. The simulation model is specified for a digital computer. A generic macro library of system elements including integrators and other dynamic elements has been made available to transcribe the AFCS design into a digital model. However, since the target application for this model is *real-time* piloted simulation which must execute within a prescribed time frame, there are some nodes within the design which have been eliminated from the model since the speed of their dynamic response cannot be accurately represented. The simulation time frame at Boeing varies from 25 to 45 msec. depending on the demands of additional utility functions that can be appended to the simulation (e.g. write data to a file). Therefore, dynamic elements such as the longitudinal filter on pitch rate feedback (first order lag with  $\tau = 0.004$  sec) have been deleted from the model. In these cases, the simulation model block diagram features a comment to point out to the user which dynamic elements have been deleted.

The simulation models for the Chinook have been drawn directly from the AFCS specification documents. However, the simulation block diagrams not only represent the control laws within the AFCS boxes but also include actuator and other mechanical control models required to fully emulate the control system from pilot stick to rotor blade motion. Furthermore, the AFCS specification only defines a single AFCS channel (AFCS units are identical with the exception of some flight director functions). Since the aircraft features dual AFCS systems, the simulation model features an integrated set of control laws for *both* systems. Simulation-specific logic is available to introduce failures into a single AFCS channel. The dual-system model does not apply to AFCS logic, where only a single copy is executed. In this manner, failures of a single channel logic network cannot be accomplished with this model. The detailed AFCS specification documents are referenced by the simulation model.

The Dual-channel AFCS is realized by appropriate replication of the control laws. In this manner, the summation of both channels is accomplished in the actuator section. Furthermore, since the simulation features "perfect" sensors, each channel is an exact replication of the other for normal operating conditions.

Therefore, unless single channel failures are to be simulated, this structure only increases simulation computing requirements. The Boeing simulation model features a complete replication of all dual functions for a full dual-channel simulation since the computing overhead is not a significant factor. The output of the AFCS and pilot controls is processed by the mechanical controls part of the simulation model.

### **4.3. Engine Model**

#### **4.3.1. General**

The RAF HC MK2 Chinook helicopter is powered by two Lycoming T55-L-712F turboshaft engines, each with an upgraded sea level standard rating of 3140 SHP maximum continuous power and 4315 SHP maximum rating. The simulation model is based on the 55-L-712 engine and its digital fuel controller. These powerplants drive the rotors through a transmission and interconnect shaft system which consists of individual right-angle engine nose boxes, a mixer transmission, synchronizer shafts, and forward and aft transmissions. The combined transmission rating is 7500 SHP. The net losses associated with electrical and hydraulic accessory packages driven off the aft transmission are approximately 225 SHP. Drive train losses through the transmissions are 1.5% of the power required at the rotor heads. A full authority digital electronic control system (FADEC) is used to govern power turbine speed through fuel flow metering. The airframe-mounted digital electronic control unit contains both a primary and back-up, reversionary channel in the event the primary channel becomes inoperative. The reversionary modes are not modeled in the simulation.

In the RAF HC MK2 Chinook simulation math model, only a single engine is modeled in detail. The response of this engine is duplicated prior to integration with the rotor interconnect/shaft dynamic system, which includes accessory losses. Single engine failures may be simulated with this model by exponentially decaying the torque output from the duplicated path to zero.

The model for the RAF HC MK2 Chinook engine is based on a map-driven model (i.e table look-ups) directly from Lycoming for the 55-L-712, which functions in concert with a detailed FADEC model from Chandler Evans.

#### **4.3.2. FADEC/55-L-712 Model Operation**

The FADEC is a highly nonlinear system with state-driven logic controlling which module actually is governing the fuel flow. This structure is based on modeling engine limits directly in the fuel control laws to avoid commands in excess of what the 55-L-712 engine can deliver. However, since the majority of flight time does not invoke these limits, there is a path which is nearly linear through the fuel control laws. This nominal fuel control path is through the Power Turbine Governor, to the NDOT Governor, to the Fuel flow metering valve drive (stepper motor). Fuel flow limiting modules include Power Available, Temperature (T4.5) Limiter, NDOT Acceleration Limit, NDOT Deceleration Limit, Maximum Fuel



Flow, and Minium Fuel Flow modules. In some instances, dynamic components in the Chandler Evans design have been deleted from the simulation model since the model was intended for real time operation (a typical time frame of 25 msec is assumed). In addition, since simulation cabs typically do not feature engine control panels, the engine condition levers (power lever) have been assumed to be in their "fly state" positions. Finally because the simulation model was intended for piloted review of handling qualities, the engine diagnostics, reversionary modes, fault detection and instrumentation modules of the FADEC have been omitted.

#### **4.4. Rotor Shaft Dynamic System Model**

The rotor shaft dynamic model represents the portion of the RAF HC MK2 simulation program that connects the engines to the aircraft rotors. The model is a second order spring-mass-damper system, featuring individual forward and aft rotor drive trains with independent rotational degrees of freedom. Accessory drive and transmission gear losses are modeled as a constant 257 SHP decrement for all flight conditions. In addition to these losses, all major drive train elements are modeled as far as their inertial and torsional contributions to overall shaft dynamic performance are concerned. Rotor and engine transmissions are considered along with major interconnect shaft elements and components. Shaft horsepower provided by one or both of the engines goes directly into the rotor shaft dynamic model.

## **5. EXTERNAL SLING LOAD**

### **5.1. General**

The Boeing bifilar tandem suspension sling load dynamics model (and its inertial and aerodynamic coupling with the basic airframe EOM) is described in this section of the report.

The basic airframe rigid body equations of motion discussed earlier have been re-derived to include the effects of combining a partially linearized external sling load dynamic response model with the basic helicopter airframe model.

When the external sling load is coupled with the airframe, three additional degrees of freedom (representing the suspension cable sway angles) are introduced. As shown in Figure 20, a typical suspended external load consists of an 8 x 8 x 20 foot MILVAN container, slung beneath the helicopter fuselage on two equal length suspension cables from hooks on the aircraft bottom (located the same distance below and equidistant horizontally from the aircraft C.G.). This tandem suspension scheme permits longitudinal, lateral and differential bifilar (yawing) motions of the load, with respect to the helicopter fuselage. Cable angular accelerations are computed and then integrated to obtain their respective angular rates and displacements, which are in turn used in the original airframe acceleration EOM.

The cable angles associated with this motion are defined as follows:

- $\mu_{SL}$  longitudinal cable angle (in X-Z plane of helicopter) defined as (+) for forward sway W.R.T. the fuselage.
- $\lambda_{SL}$  lateral cable angle (in Y-Z plane of helicopter) defined as (+) for sway to the left W.R.T. the fuselage.
- $\nu_{SL}$  lateral differential cable angle (in X-Y plane of helicopter) - defined as (+) for nose right yaw displacement of the load W.R.T. the fuselage centerline.

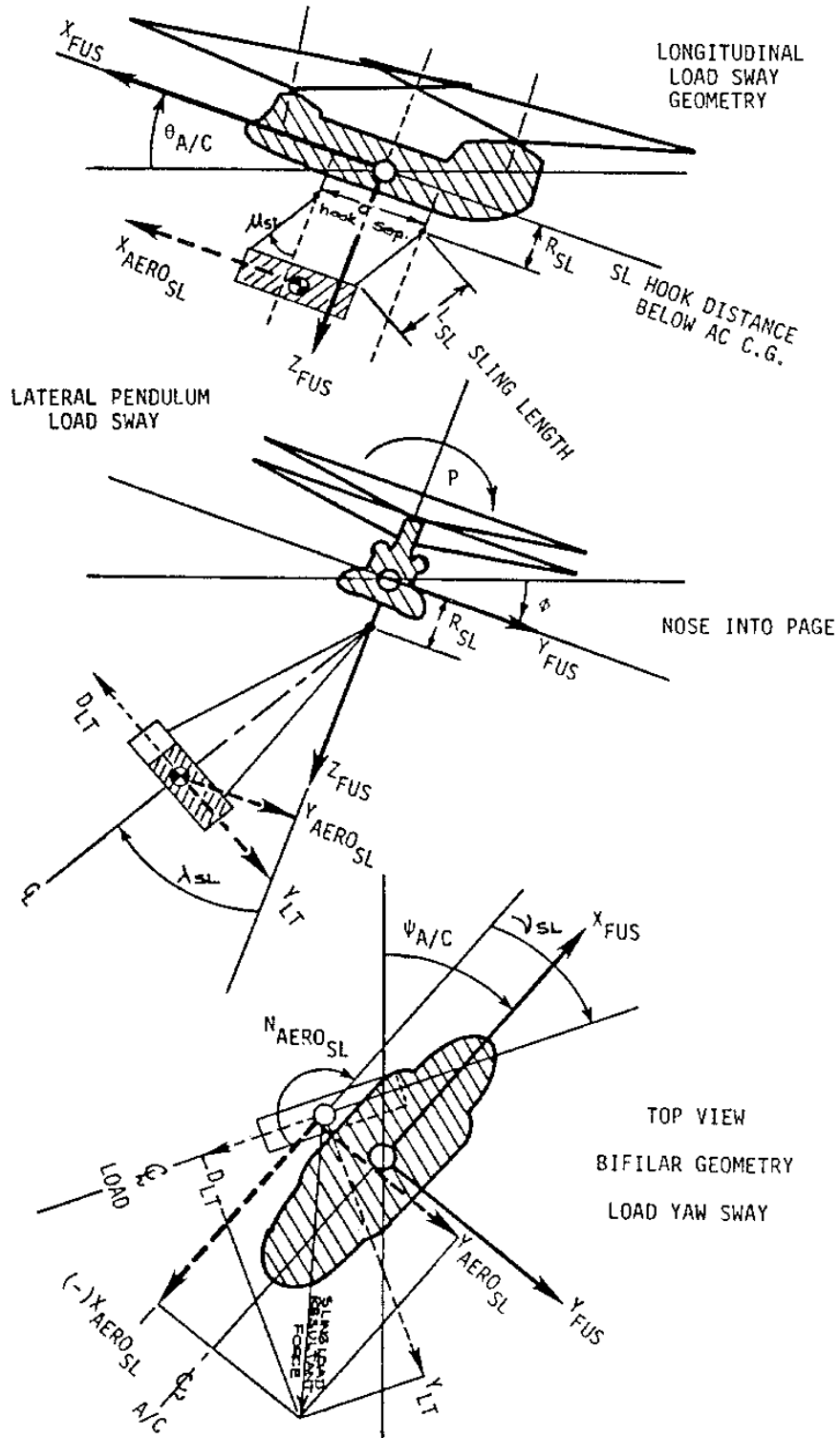


Figure 20 - External Load Geometry

## 5.2. Preliminary Calculations

As was accomplished in the airframe model, some repeating (sling load) terms have been precalculated to save computational time. A Lagrangian approach was taken in synthesizing the sling load contributions made to the basic airframe acceleration equations. In order to make the equations more tractable for real-time digital solution, a number of simplifying assumptions were made to the rather complex initial derivations. These derivations are beyond the scope of this report.

Because of cable constraints, only drag, side force, and yawing moment must be considered for the load. Aerodynamic lift and pitching moment are assumed to be small and invariant with changes in fuselage body axis longitudinal velocity and longitudinal cable angle (See Figure 21). Once the forces and moments have been determined, they are resolved through the load differential yaw angle ( $v_{SL}$ ) into the helicopter body axis for computation in the equations of motion.

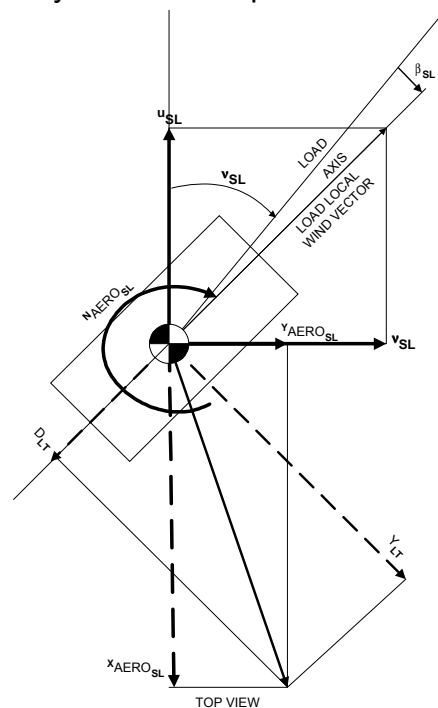


Figure 21 - Load Velocity and Force Resolution

## 6. MODEL VALIDATION DATA

In order to validate this model, batch simulation time histories were replicated of flight test maneuvers from events recorded in 1994 and 1995 at Edwards AFB in conjunction with a cooperative handling qualities test of the CH-47D between the

U.S. Army and Boeing. Data from selected maneuvers are available in an electronic version to facilitate validation and verification of the rehosting of this model by NLR.

Note, the AFCS for the flight test configuration was CH-47D, which differs from the RAF HC MK2 in some areas. Specifically, the longitudinal axis of the RAF HC MK2 AFCS features upgrades that are not available on the CH-47D. In addition, the shape of the nose on the airframe of CH-47D and RAF HC MK2 airframes differs enough to warrant a slight difference in the sideslip control laws. Therefore, for cases when the maneuvering states of the flight test aircraft entered areas of the flight envelope for which the AFCS control laws differ, the vehicle response for the simulated RAF HC MK2 should be expected to be different from that exhibited by the flight test vehicle (CH-47D). Alternatively, many of the features of these time histories are generic enough that the differences between CH-47D and RAF HC MK2 configurations are not significant.

When the flight and simulation data do not agree because the AFCS configurations were different, the time history data are important as verification cases to ascertain that the simulated AFCS features specific to the RAF HC MK2 are functioning properly in the rehosted math model.

The following data are available:

- Directional Pulse in Hover
- Longitudinal Step Input at 60 kts
- Lateral Attitude Quickness Test at 60 kts
- Lateral Reposition (Sidestep)
- Normal Departure/Abort Maneuver (Acceleration/Deceleration from Hover)
- Precision Hover Maneuver

Validation data were generated by trimming the simulation model to the initial condition for each flight test event and then driving the model with the exact controller time history from flight test. In order to accomplish this without having dissimilarities in trim further degrade the correlation, any offset between flight test and simulation model in the initial trim condition of cockpit control positions was synchronized to zero. In this manner, all of the dynamic variation of the event was replicated for the control input and the subsequent time history is always started from a trimmed state.

Deviations in the aircraft trim state between simulation and flight test may be noted by comparison of the starting values for aircraft attitudes (pitch and roll).

Note, the simulation data have been gathered in a totally open loop manner from the math model. Any deviation from the actual recorded test trajectory was not

used to drive the feedback signals for the simulation. Therefore, the correlation is considered quite high in fidelity, since the cases could typically be run through their entire duration. As noted, there are some cases where the signals are expected to deviate due to differences in AFCS control laws.

In each case the following variables (in engineering units as shown) are available to compare the simulation with flight test data:

- Longitudinal Stick – inches of stick
- Lateral Stick – inches of stick
- Directional Pedals – inches of pedal
- Collective Stick – inches of stick
- hradar (simulation radar altitude data only for comparison with flight test parameter RADALT) - feet
- h (simulation height data only for comparison with flight test parameter RADALT) - feet
- RADALT (flight test data only for comparison with the preceding simulation parameters) - feet
- Pitch Rate – degrees/sec
- Roll Rate – degrees/sec
- Yaw Rate – degrees/sec
- Pitch Attitude – degrees
- Roll Attitude – degrees
- Psideg (simulation heading data only for comparison with flight test parameter HEADING) - degrees
- Heading – degrees

The following notes clarify the references used for these variables.

The simulation variables for the cockpit controls (cyclic stick and pedals) are referenced about the center of their travel (neutral position). The flight test data are referenced with respect to full travel as follows:

Longitudinal Stick is measured with respect to inches from Full Forward (8.05 inches from neutral)

Lateral Stick is measured with respect to inches from Full Left (4.45 inches from neutral)

Pedal Position is measured with respect to inches from Full Left (3.9 inches from neutral)

In both cases, the collective stick is referenced from its full down position in inches.

In this manner, even though the exact cockpit controller time histories taken from flight test were executed by the simulation, test and simulation data do not overlay, but are biased. This offset facilitates the observation that the simulation was executing the exact test time history of controller inputs. It also illustrates where there is any deviation in the simulated initial condition of control position from the recorded flight test trim state.

The simulation model was not always initialized at the same compass heading as recorded from the flight test. Since winds were not a factor for any of the flight tests, heading offsets are insignificant.

## **7. STABILITY DERIVATIVE AND CONTROL SENSITIVITY MODEL OVERVIEW**

This model can be used to generate stability and control derivatives for 6 degree-of-freedom linear models. Derivatives are calculated by perturbing each of the state variables by a fixed amount from its trim value and then executing the entire model with all state variables held fixed except the one being assessed. The actual derivative value is then obtained taking the difference between the perturbed and trim results. Derivatives are normalized with respect to their on-axis mass (translational derivatives) or inertia (rotational derivatives).

All derivatives are computed with the AFCS, engine, and shaft dynamic models frozen in their trim states.

Results from the derivative computations are presented on the trim sheet.

## **8. AIRFRAME TRIM LOOPS**

Figure 22, schematically describes the feedback loops used in the model to trim the aircraft in the initial condition/trim mode (IC/trim). The dynamics of model elements coded in C (AFCS, FADEC, 55-L-712 engine, drive system and mechanical control system) are suspended in the IC/trim mode by holding all dynamic elements in their respective IC modes, causing the IC values of these to be passed as output. Other parts of the model (FORTRAN code) function approximately as they do when the simulation is in the operate or FLY mode, except for the loops shown in Figure 22. These loops are only closed during IC/trim and function as follows:

The three body axis angular accelerations (PDOT, QDOT, and RDOT) and the body axis vertical acceleration (WDOT) are fed from the airframe model to a series of gains and integrators, as shown in Figure 22. Each produces a trim command for the cockpit controllers (longitudinal and lateral cyclic stick, pedals and collective stick) that is sent to the control system. These signals then pass through the control system and are fed back into the airframe model as rotor commands to “fly” the model to a trimmed state. Additional feedback paths that

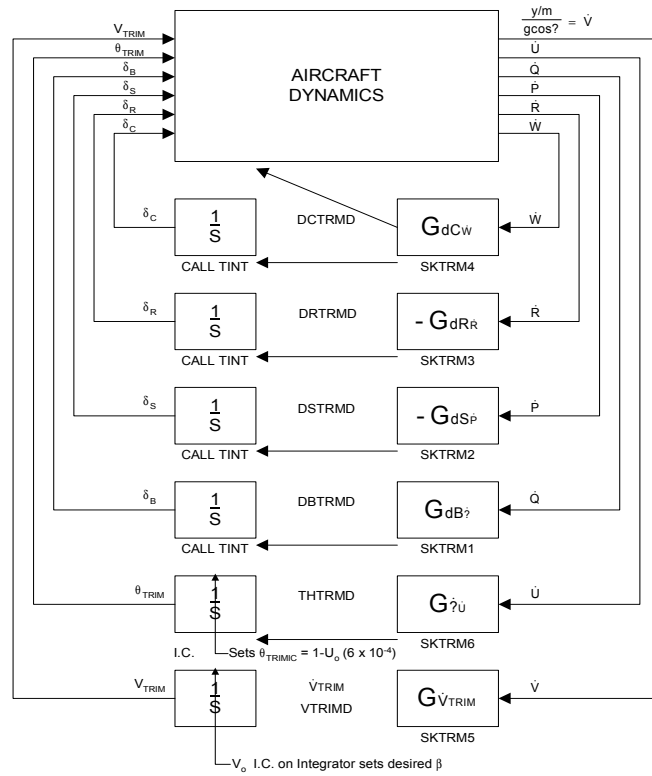
operate on longitudinal acceleration (UDOT) to trim body pitch attitude ( $\theta$ ) and lateral acceleration (VDOT) to trim sideslip ( $\beta$ ) are also included to complete the six-degree-of-freedom balance of forces and moments required for trim.

The VDOT trim loop described at the bottom of Figure 22 is derived from the aircraft lateral acceleration ( $Y_{force}/Mass$ ) divided by the appropriate gravitational component ( $g\cos(\theta_{trim})$ ) and then multiplied by an appropriate, user specified, trim gain. The VDOT trim loop uses a user-specified  $v_0$  (initial lateral velocity) which establishes a desired sideslip. In this manner, as this trim loop is integrated, the result is either a sideslip command of 0.0 or the preselected value. Once the  $V_{trim}$  value is computed, it is used as the initial condition for the VDOT equation within the air vehicle equation of motion.

The WDOT trim loop uses an analogous process to setting up a desired rate of climb by computing a  $W_{trim}$ . The computed value of  $W_{trim}$  is used as the initial condition in the WDOT equation of motion.

Note - all trim gains are adjustable by the user to optimize trim loop computational time and convergence.





For setting up desired R/C,  $W_{TRIM}$  is introduced as I.C. on  $\dot{w}$  EOM integrator.

$$W_{TRIM} = \frac{-\dot{h}_{TRIM} + u_0(\sin \theta_{TRIM}) - V_{TRIM}(\sin \phi_{TRIM} \cos \theta_{TRIM})}{(\cos \phi_{TRIM})(\cos \theta_{TRIM})}$$

For setting trim  $\beta = 0$ ,  $V_{TRIM}$  is introduced as I.C. on  $\dot{v}$  EOM integrator.

$$\dot{V}_{TRIM} = \frac{G \frac{Y}{m}}{g \cos \theta_{TRIM}} \qquad \int \dot{V}_{TRIM} = V_{TRIM}$$

$$\frac{V_{TRIM}}{U} = \beta$$

IF  $\beta = 0$ ,  $V_{TRIM}$  MUST BE 0

Figure 22 - Math Model Trim Loops

## **9. REFERENCES**

1. Gessow, A. and Meyers, G.; "Aerodynamics of the Helicopter," Copyright 1952, Reprinted 1967, 1978, Frederick Ungar Publishing Co. N.Y., N.Y.
2. NASA Ames Contract - NAS2-11136, "Mathematical Model of the CH-47B Helicopter Capable of Real-Time Simulation of the Full Flight Envelope," 1 December 1981
3. Etkin, B., "Dynamics of Atmospheric Flight," copyright 1972 - John Wiley & Sons Inc., N.Y., N.Y. London, Sydney, Toronto
4. Thelander, J. A., "Aircraft Motion Analysis," U.S. Air Force Report, FDL-TDR-64-70, dated March 1965

## DESCRIPTION OF TANDEM ROTOR HELICOPTER TRANSIENT ANALYSIS PROGRAM B-29

### DESCRIPTION

The Boeing tandem helicopter transient analysis (B-29) is a digital computer program which is capable of examining in depth the details of rapid helicopter maneuvers over a short period of time (up to 20 sec). However, real-time capability has not been implemented for this program, and hence it is not suitable for piloted simulations. All results are presented as digital printout, which can then be plotted using standard graphics packages. The program incorporates the following capabilities and features.

- Rotor blade element analysis (20 blade azimuths, 9 radial stations).
- Rotor airfoil stall characteristics.
- Mach number effects on rotor blade aerodynamic characteristics.
- Effects of rotor inflow lag and blade radial flow.
- First order representation of engine response characteristics.
- Second order AFCS modeling suitable for all CH-47D/HC Mk2 AFCS channels.
- Blade lead/lag motion representation.

The blade element analysis incorporates the following basic assumptions: (a) uniform air inflow is assumed over the rotor disks, and (b) rotor blades are assumed inflexible in bending and torsion.

The aerodynamic lift and drag characteristics of the rotor blade airfoil sections are represented by two dimensional tables in terms of angle of attack and Mach number, for angles of attack between +/-20 deg. For angles of attack beyond +/-20 deg, representative equations are used. It is by means of these tables and equations that airfoil stall and Mach number effects are incorporated in the analysis. The static lift and drag data in these airfoil tables are then modified by equations which represent the effects of the oscillatory angle of attack variations encountered by the blades as they rotate about the hub (alpha dot effect), and the radial airflow components which occur primarily in the forward and aft rotor disk quadrants due to the forward velocity of the helicopter (sweep effect).

The first order engine response representation may not be adequate when rapid collective control inputs are an important feature of the overall aircraft response. In such cases, the computed response of the aircraft with the simple first order engine control model can be determined, the computed response of the actual engine control system (e.g. FADEC) can be independently defined for the same control inputs, and the difference between the two engine responses can be added as a torque increment to the simple first order engine response, during a second running of the same flight case.

The aerodynamic force and moment characteristics of the fuselage are represented by two dimensional tables in terms of angle of attack and sideslip, for angles up to +/-180 deg. The data in these tables were obtained by wind tunnel tests on a CH-47B model fuselage.

Aerodynamic interference effects generated by the downwash of the rotors on each other and on the fuselage are represented by third order equations based on theory and test data.

### OPERATION

The program first trims the helicopter at the specified initial conditions (gross weight, center of gravity, airspeed and altitude). Initial conditions may include a steady rate of climb and/or sideslip. Control inputs are then introduced in tabular format vs time, and the program computes the resultant responses in terms of

- Airspeed, altitude, distance traveled, normal force and climb angle.
- Fuselage attitudes, rotor RPM and engine torque output.
- Rotor thrust, inplane forces, hub moments and torque required.
- Individual rotor collective and cyclic pitch variations.
- All AFCS activity.
- Individual blade flap, lag and pitch angles.

Results are available in terms of a tabulated printout, from which time records of any combination of output parameters can be constructed, using standard graphics packages.